CONTRACT NO. NAS 9-15796

FINAL REPORT

by

David L. Cooke

and

John W. Freeman

Department of Space Physics and Astronomy
Rice University
Houston, Texas 77001

for
NASA Johnson Space Center
Houston, Texas 77058

(NASA-CR-160796) A COMPUTER MODEL OF SOLAR PANEL-PLASMA INTERACTIONS Final Report (Rice Univ.) 59 p HC A04/MF A01 CSCL 10A

N80-32853

Unclas
G3/44 28796

CONTRACT NO. NAS 9-15796

FINAL REPORT

by

David L. Cooke

and

John W. Freeman

Department of Space Physics and Astronomy
Rice University
Houston, Texas 77001

for
NASA Johnson Space Center
Houston, Texas 77058

(NASA-CR-160796) A COMPUTER MODEL OF SOLAR PANEL-PLASMA INTERACTIONS Final Report (Rice Univ.) 59 p HC A04/MF A01 CSCL 10A

N80-32853

Unclas
G3/44 28796

TABLE OF CONTENTS

ABSTRACT

"A Computer Model of Solar Panel-Plasma Interactions"

High-power solar arrays for satellite power systems are presently being planned with dimensions of kilometers, and with tens of kilovolts distributed over their surface. Such systems will face many plasma interaction problems, such as power leakage to the plasma, particle focusing, and anomalous arcing to name a few. In most cases, these effects cannot be adequately modeled without detailed knowledge of the plasma-sheath structure and space charge effects. This report details the work performed under contract NAS 9-15796 to adapt the computer program PANEL to augment the laboratory studies of a 1 x 10 meter solar array in a simulated low Earth orbit plasma being conducted in the chamber A facilities at NASA/Johnson Space Center. The plasma screening process is discussed, program theory is outlined, and a series of calibration models is presented. These models are designed to demonstrate that PANEL is capable of accurate self-consistent space-charge calculations. Such models include PANEL predictions for the Child-Langmuir diode problem. Also included are two models of the interactions of an infinitely long one meter wide solar array in a dense, 10 eV plasma.

1: INTRODUCTION

The interaction of a large high voltage solar array with a space or laboratory plasma cannot, in general, be modeled analytically. For this reason, a computer program, PANEL, has been developed to calculate potentials, densities, and currents on a three-dimensional grid of points. A major feature of PANEL is that it includes space-charge effects in a self-consistent manner. The method used in PANEL is an extension to three dimensions of the inside-out method developed by Parker (1964), and used by Parker and Whipple (1970) to model two-electrode probes on a satellite. More recently Parker (1976, 1977a) has used the method to calculate sheath and wake structures about disk and pill-box shaped objects in flowing plasmas. An early version of PANEL, written by Parker (1977) was used by Reiff, Freeman, and Cooke (1980) to model the interaction of a geosynchronous substorm plasma with the NASA/Marshall Space Flight Center baseline design for the solar power satellite (Hanley, 1978). The purpose for the further development of PANEL, reported here, has been to produce a code capable of augmenting the laboratory studies of a 10 meter solar array in a simulated low Earth orbit plasma being conducted at NASA/Johnson Space Center (McCoy and Konradi, 1978).

Section 2 of this report contains a general discussion of the plasma screening process, applications of the Child-Langmuir diode law, and a development of an analytic model for comparison to PANEL results. Section 3 describes the inside-out method as it is used in PANEL to solve the coupled Vlasov-Poisson equations in two- and three-dimensions. And in section 4, current PANEL results are presented. Appendix A contains a review of the symbols and units used in this report. Appendix B gives a subroutine linkage chart, and Appendix C outlines the modifications to PANEL for the two-dimensional option. The emphasis so far, has been on testing PANEL against the

analytic models discussed in section 2. Also included are two two-dimensional models of an "infinitely long" charged panel.

2: THE PLASMA SHEATH

Perhaps the best known example of plasma screening is the Debye treatment of the plasma screening of an isolated test charge. A positive test charge, δQ, placed in a plasma of temperature T, will attract electrons and repel ions so as to develop a surrounding sheath with a potential distribution given by,

$$V(r) = \frac{\delta Q}{4\pi\varepsilon_0 r} \exp\ (-r/\lambda_D)$$

where $\lambda_D = (\varepsilon_0 kT/N_0 e^2)^{1/2}$ is the Debye length. Implicit in the derivation of this equation (Jackson, 1962) are the assumptions that the charge has negligible cross-section, and that $V(r) \ll kT/e$ for $r > \lambda_D$. For a microscopic body of radius R, satisfying these assumptions, we can write

$$V(r) = \frac{V_b\ R}{r} \exp\ (-r/\lambda_D) \qquad (2\text{-}1)$$

where V_b is the surface potential of the body.

For macroscopic bodies with a high degree of symmetry, sheath structures may be calculated by capitalizing on the constants of the motion allowed by the symmetry, e.g., angular momentum (Whipple, 1977). In general though, self-consistent treatment of a macroscopic body requires computer modeling. In spite of this difficulty, a better understanding of the shielding process can be gained by studying current limiting by space charge in the 1-D planar

electron diode.

The first theoretical treatments of the electron diode were published independently by Child (1911) and Langmuir (1913). Variations on this problem have been studied by Fay et al. (1938), and the general topic of space charge effects in vacuum tubes is treated in the book by Birdsall and Bridges (1966).

Consider the three electrode system shown in Figure 2/1. At $x = -d$, we have a cathode, with zero potential capable of emitting unlimited quantities of electrons all with zero velocity. At $x = 0$, we have a transparent screen at potential V_0, and at $x = x_1$, we have a non-emitting anode at potential V_1. The kinetic energy of an electron at x is

$$\frac{1}{2} m_e v^2 = eV. \tag{2-2}$$

The current density for electrons at x is

$$J = \rho v \tag{2-3}$$

where ρ is the charge density. Poisson's equation in one dimension is

$$\frac{d^2V}{dx^2} = -\rho/\varepsilon_0. \tag{2-4}$$

Substituting for ρ from equation (2-3) and then for v from equation (2-1), we have

$$\frac{d^2V}{dx^2} = -\frac{J}{\varepsilon_0}\left(\frac{m_e}{2eV}\right)^{1/2}. \tag{2-4}$$

Multiply this by $2\frac{dV}{dx}$ and integrate from $(0, V_0)$ to (x, V_x);

$$\left(\frac{dV}{dx}\right)^2 \Big|_0^x = -\frac{J}{b^2} \cdot \frac{16}{9}\left(V_x^{1/2} - V_0^{1/2}\right) \tag{2-5}$$

where $b^2 = \frac{4\varepsilon_0}{9}(2e/m_e)^{1/2} = 2.336 \times 10^{-6}$ (amps/volts$^{3/2}$). The boundary condition that we desire at $x = 0$, is $E_x = -\frac{dV}{dx}\Big|_0 = 0$, a common definition of the

sheath edge in the spacecraft charging problem. Using this condition, and taking the positive square root of equation (2-5),

$$\frac{dV}{dx} = \frac{4}{3b}\left[J_e\left(V_x^{1/2} - V_0^{1/2}\right)\right]^{1/2} \tag{2-6}$$

where $J_e = -J$. Solving for dx we integrate again from $(0, V_0)$ to (x_1, V_1);

$$x_1 = \frac{b}{\sqrt{J_e}} V_1^{3/4}\left[1 + 2\left(\frac{V_0}{V_1}\right)^{1/2}\right] \cdot \left[1 - \left(\frac{V_0}{V_1}\right)^{1/2}\right]^{1/2}. \tag{2-7}$$

This equation can be applied to region I, $-d < x < 0$, where $V_0 = 0$ (zero initial velocity) to recover the Child-Langmuir (C-L) result

$$d^2 = 2.336 \times 10^{-6}\, V^{3/2}/J_e, \tag{2-8}$$

where d^2 and J_e must have the same unit of area. If d and V are fixed, equation (2-8) gives the maximum conducted current despite an unlimited supply of electrons. If d, V, and J_e are all considered independent, the sheath edge electric field that was set to zero will become the dependent variable.

To apply equation (2-7) to a planar spacecraft surface at potential V, we identify x_1 with the spacecraft surface, and $x = 0$ with the sheath edge where $E = 0$. Region I is now identified with the undisturbed plasma where V_0 represents the average thermal energy of the electrons. Therefore, a transformation of voltage is needed because we want the sheath edge to be at zero potential; thus, $V_1 \rightarrow V + V_0$

define $$\psi = \frac{V}{V_0} = \frac{V_1 - V_0}{V_0} = \frac{V}{kT_e},$$

and $$\frac{V_0}{V_1} = (\psi + 1)^{-1}. \qquad (2\text{-}9)$$

Substituting this last result into equation (2-7) we get for the sheath thickness a,

$$x = a = b\,(V^{3/4}/\sqrt{J_e}) \cdot S(\psi) \qquad (2\text{-}10)$$

$$S(\psi) = \{(1 + \psi^{-1})^{3/4} \cdot [(1 + 2\,(1 + \psi)^{-1/2}) \cdot (1 - (1 + \psi)^{-1/2})^{1/2}]\}. \qquad (2\text{-}11)$$

Equation (2-10) is written such that $S(\psi)$ is the correction to the usual Child-Langmuir result due to non-zero initial velocities. Equation (2-11) is plotted in Figure 2/2 as a function of log (ψ^{-1}). When applied to a Maxwellian plasma, $S(\psi)$ will be only qualitatively correct since there will be a distribution of initial velocities, but it should be reasonably accurate for larger values of ψ.

Another variation of this problem is given by Birdsall (1966). The conditions are illustrated in the lower portion of Figure 2/1, with the grids at $x = 0$ and x_1 both at the same positive potential V_1, and the separation distance x_1 considered fixed. The negative space charge of the electrons in the gap between zero and x_1 will depress the potential in the gap and give rise to current limitation if the potential drops to zero. This variant is more suited for comparison to PANEL, since the geometry is fixed and only voltages and charge densities vary. The potential distribution in the gap is determined by subdividing region II into regions A and B whose boundary at x_m is the point of minimum potential where we have also the condition of zero electric field. The potential can be obtained separately in each region with exactly the same approach that led to equation (2-7) to give

$$b[(2 - f)\,J]^{-1/2} \cdot (V_A^{1/2} + 2V_m^{1/2}) \cdot (V_A^{1/2} - V_m^{1/2})^{1/2} = x_m - x_A$$

$$b(fJ)^{-1/2} \cdot (V_B^{1/2} + 2V_m^{1/2}) \cdot (V_B^{1/2} - V_m^{1/2})^{1/2} = x_B - x_m \qquad (2\text{-}12)$$

The factor, f, is the fraction of transmitted current; if $V_m > 0$, $f = 1$. Equations (2-12) may be solved for x_m by setting $(V_A, x_A) = (V_1, 0)$ and $(V_B, x_B) = (V_1, x_1)$. For the case $V_m > 0$ and $f = 1$, we find $x_m = x_1/2$, and equations (2-12) can be combined to give Birdsall's equation:

$$(\phi^{1/2} - \phi_m^{1/2})\,(\phi^{1/2} + 2\phi_m^{1/2})^2 = \beta(\xi - 1/2)^2 \qquad (2\text{-}13)$$

where $\phi = V/V_1$, $\phi_m = V_m/V_0$ and $\xi = x/x_1$. The dimensionless current β, is defined by $\beta = J_e/b^2\, V_1^{3/2}\, x_1^{-2}$, where the normalizing current is C-L current for a diode with separation x_1, and potential drop V_1. The value of the minimum potential for a given current is found by evaluating equation (2-13) at $x = 0$, giving

$$4\phi_m^{3/2} - 3\phi_m^{1/2} + (\tfrac{\beta}{4} - 1) = 0. \qquad (2\text{-}14)$$

Figure 2/3a (from Birdsall) gives ϕ_m as a function of input current β. The dotted portion of the curve, has been labeled the "C-overlap" by Fay et al. (1938) and has been shown to contain no stable solutions (Birdsall, 1966). Figure 2/3b (also from Birdsall) gives selected potential profiles from equation (2-13) for the range $0 < \beta < 8$.

For solutions with $\beta > 8$ we set $\xi_m = 0$ in equation (2-12). Allowing now for $f < 1$ and a non-symmetric potential distribution, we can derive Birdsall's dimensionless equations;

$$\phi_A^{3/2} = (2 - f)\,\beta\,(\xi - \xi_m)^2$$

$$\phi_B^{3/2} = f\beta\,(\xi - \xi_m)^2, \tag{2-15}$$

$$\xi_m = \frac{[f\,(2 - f)]^{1/2} - f}{2(1 - f)}\,, \tag{2-16}$$

$$\beta = 2\,\left[\frac{[f\,(2 - f)]^{1/2} + 1}{f\,(2 - f)}\right] \tag{2-17}$$

where $\xi_m = x_m/x_1$. Figure 2/3c (also borrowed from Birdsall), shows a few selected potential profiles from equations (2-15).

The multiplicity of solutions in the region $4 < \beta < 8$ means that there should be hysteresis in the behavior of the classical diode model. This hysteresis was observed experimentally by Gill (1925). He also observed the predicted current limiting. It should be mentioned that although the condition $V_m = 0$ does lead to mathematical solutions for the range $4 < \beta < \infty$ these solutions are a result of the enforced time-independence of the classical method and can be shown to be unstable when time dependence is considered (Birdsall, 1966). This lack of stability has been confirmed by the experiments of Salzberg and Haeff (1938).

These solutions of what I call the gap problem have been very useful in the development of PANEL. PANEL's predictions for the gap model will be presented in section 4.

Returning now to the spacecraft plasma sheath problem, it is common to use the C-L sheath thickness given in equation (2-8) as an estimate of satellite sheath thickness for appropriate conditions. These conditions are:

1. Satellite dimensions should be much larger than all estimates of sheath thickness, such that a planar approximation is justified.

2. The surface potential is much greater than the plasma temperature, so the initial velocities of particles entering the sheath can be neglected [or accurately accounted for by equation (2-10)]. Also repelled particles must not penetrate significantly into the sheath since the C-L treatment considers only attracted particles.

3. The current is assumed to be the random thermal current ($J_0 = N_0 e \sqrt{kT/2\pi m}$) of attracted particles falling on the sheath edge.

For diode geometries other than planar, Langmuir (1913) has shown that the space charge limited current will always be proportional to $V^{3/2}$, however, the distribution of potential in space does depend on geometry. The problems of current flow between concentric spheres and cylinders has been addressed by Langmuir and Blodgett (1924). Their solutions take the form of equation (2-8) with d replaced by various series expansions in terms of the ratios of the electrodes' radii, with the results presented in tabular form. Parker (1979) has adapted these results to estimate sheath thickness for charged spherical satellites, and provides a convenient fit to those results. In the following equations a = sheath radius, r_0 = body radius, and d is the C-L screening distance given by equation (2-10) with $\psi = \infty$, or by equation (2-20) below:

$$\frac{a}{r_0} = \begin{cases} \frac{1}{2} + \left[\frac{1}{4} + \frac{d}{r_0}\right]^{1/2} & ; \frac{d}{r_0} < .2 \\ \frac{1}{2} + \left[\frac{1}{4} + \frac{d}{r_0}\right]^{1/2} + 0.052\,\frac{d}{r_0} & ; .2 < \frac{d}{r_0} < 19 \\ \left[1 + \left(\frac{d}{r_0}\right)^{.753}\right]^{.7524} = \left(\frac{d}{r_0}\right)^{.567} & ; \frac{d}{r_0} > 19 \end{cases} \qquad (2\text{-}18)$$

It is interesting to stop at this point and compare screening length estimates. On one hand, we have the Debye length for the microscopic case with low potentials

$$\lambda_d = [\frac{\epsilon\, kT}{N_o e^2}]^{1/2} \text{ meters} \qquad (2\text{-}19)$$

and, on the other hand, the planar C-L screening length

$$d_{cl} = \frac{2}{3} (\frac{4\pi e \epsilon_o^2}{N_o^2 kT})^{1/4} V^{3/4} = 9.34\ (T(ev))^{-1/4} \cdot N_o(cm^{-3}))^{-1/2} V^{3/4} \text{ meters} \qquad (2\text{-}20)$$

where I have substituted for the current the thermal current J_o. Note the difference in the temperature and density dependencies; $(T/N)^{1/2}$ as opposed to $(N^2T)^{-1/4}$. A brief example will help demonstrate the inappropriateness of applying the Debye model to large objects. Consider an object of radius r_o = 10m, at a potential of 100V in a plasma with T_e = 1 ev, and N = 100/cc. For these conditions, the C-L distance is by (2-20), d = 29.5 m, and from (2-18) we have a = 2.4 r_o = 24m; whereas with a Debye length of 0.74 m, equation (2-1) predicts a = 13 m for a sheath edge potential of one volt. The Debye model predicts screening on the order of a few Debye lengths which significantly underestimates the sheath thickness.

The planar, one-dimensional C-L screening length has its own shortcomings. In applying it to space conditions one assumes that the screening length will be small compared to surface dimensions so that the surface can be approximated as infinite. But this is incompatible with the assumed boundary condition of an undisturbed plasma one screening length away from the surface. Since repelled particles will be reflected at the sheath edge, the repelled particle distribution will be nearly isotropic. On the other hand, the

attracted particles come to the edge from one direction only, resulting in only a hemispherical distribution out to a point where the surface no longer appears infinite. Such a plasma cannot even be quasi-neutral unless the potential at the "sheath edge" is significantly non-zero, which would be contrary to the original conditions of the C-L model. This difficulty is not as severe for the cylindrical and spherical extensions. This situation can be improved somewhat if we relax the definition of the sheath edge to require only that the electric field be near zero there, and let the potential deviate from zero (closer to the surface potential) so as to draw in more attracted particles and reduce the repelled particle density. This in turn requires that we invoke a presheath region to match the sheath edge to regions where the attracted and repelled distributions are identical, and the potential and electric fields vanish.

This presheath problem was recognized and accounted for by Langmuir (1929) in his analysis of a plasma discharge between plane parallel electrodes, however the resolution of that problem is too involved for presentation here, and not directly applicable to the problem of a planar satellite in a collisionless plasma. The presheath problem has also been studied by Parker (1980) for an extremely large spherical body (large compared to all estimates of sheath thickness) in a collisionless plasma, using a technique similar to the inside-out method but solving a condition of quasineutrality instead of Poisson's equation. The sheath was modeled as a potential discontinuity at the surface. Results indicate that no matter how thin the sheath gets, the presheath thickness will always be comparable to body dimensions (as one would expect from geometrical shadowing considerations). In the presheath region the potential drop is of order kT/e and the

ion and electron densities are essentially equal, but reduced from ambient values. One-dimensional theory predicts that such a body will collect a current density of attracted particles equal to the random thermal density current, but a conclusion of Parker's study was that the collected current density will be increased in the presheath region by a factor dependent upon the body potential but approaching a limiting value of 1.45 for infinite body potential, independent of body shape.

Another complication is presented by secondary and photoelectron emission. The extent to which these additional sources will modify a plasma sheath is of course dependent upon the emission flux. Guernsey and Fu (1970) and Fu (1971), have studied the case charactarized by $(N_\upsilon/N_e) > (T_e/T_\upsilon) > 1$ where the υ subscript refers to the photo or secondary electrons, and the e for the plasma electrons. We would expect these conditions to lead to a positive surface potential of a few volts and a monotonic decrease to zero with increasing distance from the surface. Their study confirmed that solution, but also revealed the existence of another non-monotonic type with a negative "overshoot" potential minimum located about one photoelectron Debye length from the surface. This overshoot was also accompanied by a lowering of the equilibrium surface potential by an amount roughly equal to the overshoot potential. Without a time dependent analysis one cannot decide which solution is the true steady-state, but energy considerations suggested that the non-monotonic solution is the true steady-state when $\frac{N_e}{N_\upsilon}\left(\frac{H_\upsilon}{4\pi kT}\right) < 1$, where H_υ is the peak in the photoelectron kinetic energy spectrum.

If the preceeding picture of the plasma screening process seems incomplete, it is for a few good reasons. One is that many aspects of the problem have not been fully investigated yet, but more importantly, there are just too many parameters to ever hope to develop a "one-size fits all" theory of plasma

screening. In my opinion, the objectives of this line of research is to develop the necessary methods and computational tools to solve specific problems as they arise.

3: THE INSIDE-OUT METHOD

The classical theory of electrodynamics states that the scalar electrostatic potential $V(\vec{x})$ and the charge density $\rho(V(\vec{x}))$ will satisfy Poisson's equation

$$\nabla^2 V(\vec{x}) = -\rho(V(\vec{x}))/\varepsilon_0. \tag{3-1}$$

In problems where the charge density does not depend upon the potential, equation (3-1) becomes an inhomogeneous linear elliptic partial differential equation. For such equations, the theory of partial differential equations (Jackson, 1962), will guarantee a unique solution interior to a closed boundary S, on which is specified either (but not both) the potential $V(\vec{x}_s)$ (Dirichlet boundary conditions), or the normal derivative $\partial V(x_s)/\partial \hat{n}_s$ (Neuman boundary conditions). Unique solutions may also be obtained for problems with mixed boundary conditions with Dirichlet conditions on part of the boundary, and Neuman for the rest. For the general non-linear problem where the charge density depends on the distribution of potential, there are no uniqueness or existence guarantees for solutions to equation (3-1). Experience, however, leads us to believe that the physically real problems that we encounter in the study of plasma screening do have at least one self-consistent solution for V and ρ. It is this experience that leads us to pursue solutions to such problems.

The inside-out method adopts an iterative approach to solving plasma sheath problems. The best estimate for $\rho(\vec{x})$ is used in equation (3-1) to obtain a new estimate for $V(\vec{x})$. Next, new estimates for $\rho(\vec{x})$ are obtained via the Vlasov equation and the latest values for $V(\vec{x})$ and the process repeated. The calculation of $\rho(\vec{x})$ has been labeled the "Vlasov problem" and the problem of finding solutions to (3-1) is called the "Poisson problem".

PANEL has the feature of being able to operate in both a two-dimensional and a three-dimensional mode. The three-dimensional version is presented first, and the conversions to two-dimensional operation are found in Appendix C.

THE POISSON PROBLEM

With $\rho(\vec{x})$ temporarily considered known and independent of $V(\vec{x})$, equation (3-1) becomes linear, thus a well posed boundary value problem will have a unique solution. PANEL uses a standard finite-difference method to solve Poisson's equation (Collatz, 1960). The approach is to discretize the space to be modeled by constructing a three-dimensional grid of points $P_{i,j,k}$. An x-y plane at constant z is illustrated in figure 3/1. The standard approach is to let the x, y, and z spacings all be a constant h so that there is a cube of volume h^3 associated with each interior point. But, in modeling many objects it is convenient to use variable spacing to achieve greater economy by allowing a higher density of points where a need is anticipated. This means that each interval must be calculated, but the symbol h will still be used to represent a typical interval. With variable spacing, the volume associated with a point P becomes a rectangular parallelepiped with faces located at the midpoints between P and its neighbors. The shaded area in figure 3/1

represents the x-y projection of this volume. Also indicated in the figure is the sense of the directions represented by the notation, N, S, E, W, U, D for north, south, east, west, up, and down, respectively.

On this grid, we now develop a difference equation to aproximate (3-1). We start with the central difference operator, δ, which is defined as

$$\delta f(x) = f(x + h/2) - f(x - h/2).$$

Applying this operator twice we get,

$$\begin{aligned} \delta^2 f(x) &= \delta [f(x + h/2) - f(x - h/2)] \\ &= [f(x + h) - f(x)] - [f(x) - f(x - h)] \\ &= f(x + h) - 2f(x) + f(x - h). \end{aligned} \tag{3-2}$$

The connection between this last expression and the second derivative can be observed by first writing the Taylor series for $f(x \pm h)$,

$$f(x \pm h) = f(x) \pm h \frac{df}{dx}(x) + \frac{1}{2!} h^2 \frac{d^2f}{dx^2}(x) \pm \frac{1}{3!} h^3 \frac{d^3f}{dx^3}(x) \pm \cdots\cdots \tag{3-3}$$

substituting these series into (3-2), we find

$$\begin{aligned} \delta^2 f(x) &= f(x + h) - 2f(x) + f(x - h) \\ &= 2[h^2 \frac{1}{2!} \frac{d^2f}{dx^2}(x) + \frac{1}{4!} h^4 \frac{d^4f}{dx^4}(x)] + O(h^6), \end{aligned} \tag{3-4}$$

and solving for $\frac{d^2f}{dx^2}$,

$$\frac{d^2f}{dx^2} = \frac{\delta^2 f(x)}{h^2} - \frac{h^2}{12}\frac{d^4f}{dx^4} + O(h^4). \qquad (3\text{-}5)$$

The simplest approximation that we can make for the second partial derivative is thus,

$$\frac{\partial^2 f(x,y,z)}{\partial x^2} = \frac{f(x + h, y,z) - 2f(x,y,z) + f(x - h,y,z)}{h^2}, \qquad (3\text{-}6)$$

with an error of order h^2. Higher order approximations can be obtained by a similar Taylor series analysis (Collatz, 1960), but the resulting formulas sufficiently complicate the consideration of boundary conditions enough to discourage their use in favor of just reducing h as much as possible. This of course increases the number of points required to model a given object; so if a machine size limit is reached and greater accuracy is still required, the use of higher order approximations would be an option.

To investigate the effect of using variable spacing we can let $h \to h_+, h_-$ where both are positive numbers. Starting again at (3-3) with this change, we see that the odd order contributions to (3-4) no longer cancel, thus (3-5) becomes

$$\frac{d^2f}{dx^2} = \frac{2\delta^2 f}{(h_+^2 + h_-^2)} - \frac{2(h_+ - h_-)}{(h_+^2 + h_-^2)}\frac{df}{dx}(x) - \cdots\cdots \qquad (3\text{-}7)$$

so, if h_+ and h_- are not nearly equal, accuracy will be reduced.

We could now formally construct a differenced form of Poisson's equation from (3-6), however it is more honest to present PANEL's Poisson algorithm as originally developed by Parker (1977b). We first throw Poisson's equation into partially dimensionless form by dividing by kT/e, so with $\Phi = Ve/kT$ and $\lambda_D^2 = \varepsilon_0 kT/N_0 e^2$ we get

$$\nabla^2\phi(\vec{x}) = \lambda_D^{-2}(n_e - n_i) = R, \tag{3-8}$$

where n_e and n_i are the electron and ion densities in units of the ambient density N_0. Integrate now (3-8) over the cell volume associated with point P, and apply the divergence theorem to the left hand side;

$$\iiint \nabla^2\phi d^3x = \oint_S \frac{\partial\phi}{\partial n} ds = \iiint R\, d^3x = Q, \tag{3-9}$$

where $\frac{\partial\phi}{\partial n}$ is the outward normal derivative at the surface of the cell. Q can be identified as the net charge within the cell, however, this identification is not implicit in the formal development. We next approximate the surface integral in (3-9) by the sum:

$$\sum_F A_F\left(\frac{\partial\phi}{\partial n}\right)_F \equiv Q, \tag{3-10}$$

where F = N, S, E, W, U, D, and A_F is the area on each of these faces. These areas are given by,

$$\begin{aligned} A_N = A_S &= \tfrac{1}{4}(x_{i+1} - x_{i-1})((z_{k+1} - z_{k-1}) \\ A_E = A_W &= \tfrac{1}{4}(y_{j+1} - y_{j-1})\,(z_{k+1} - z_{k-1}) \\ A_U = A_D &= \tfrac{1}{4}(x_{i+1} - x_{i-1})\,(y_{j+1} - y_{j-1}). \end{aligned} \tag{3-11}$$

The partials $\left(\frac{\partial\phi}{\partial n}\right)_F$ are approximated by the difference quotients:

$$\left(\frac{\partial\phi}{\partial n}\right)_N = \frac{\phi_N - \phi}{y_{j+1} - y_i}, \left(\frac{\partial\phi}{\partial n}\right)_S = \frac{\phi_S - \phi}{y_j - y_{j-1}}, \tag{3-12}$$

and similarly for the E, W, U, and D directions, where Φ is the potential at the point P, and Φ_N, Φ_S, etc. are the neighboring potentials. Thus substituting equations (3-11) and (3-12) into (3-10) we obtain the algebraic expression,

$$C_N\Phi_N + C_S\Phi_S + C_E\Phi_E + C_W\Phi_W + C_U\Phi_U + C_D\Phi_D - C\Phi = Q, \qquad (3\text{-}13)$$

where

$$C_N = \frac{(x_{i+1} - x_{i-1})(z_{k+1} - z_{k-1})}{4(y_{i+1} - y_i)},$$

and likewise for C_S through C_D; $C = \sum_F C_F$.

Equation (3-13) can be applied to each interior point in the model, but exterior or boundary points require a modified treatment so as to include the required boundary conditions. The types of boundary conditions (B.C.) used in PANEL are:

1. Floating, where the outward normal derivative on the cell and model boundary is linearly related to the potential on the boundary†.

---

†In the theory of boundary value problems, independent specification of the normal derivative and potential is an over specification of the boundary conditions and there will be no solution unless the solution was already known and used to specify the B.C. Here we are specifying only a relation between the two conditions, but even this implies a knowledge of the Green function for the problem. For the case where the boundary is far enough away from the "object" for the object to look like a point charge or at least a uniformly charged sphere, we can assume a Green function of 1/r, so we have the relations:

$$\frac{\partial\Phi}{\partial n} = \hat{n} \cdot \vec{\nabla}\Phi = \frac{-\hat{n} \cdot \vec{r}}{r^2}\,\Phi.$$

For a closer boundary, the possibility exists for finding the appropriate Green function, but this has not been pursued far enough to produce a useful algorithm.

---

2. Neuman, where the inward normal component of the electric field is specified.

3. Dirichlet, where the boundary potential is specified.

4. Extended Dirichlet, where a boundary potential of zero is assumed to exist one interval beyond the usual model boundary.

5. Reflection, where like condition 4, an extended boundary is assumed, but with a potential equal to the nearest interior neighbor.

When a boundary is assumed to represent "infinity", i.e. a source of undisturbed plasma at zero potential, the boundary should be far enough away from the "object" that all boundary conditions give the same results. It is frequently not possible to make grids that large so it becomes necessary to choose the B.C. which best approximates "infinity" on a limited grid. Parker and Sullivan (1969) has addressed this problem, and concluded that for the spherical diode problem, the floating B.C. (1) produced the best "infinity" approximation with the least computing time. The zero gradient B.C. (2) produced an effective infinity at a distance comparable to the floating B.C., but required about twice the computing time as B.C. (1). The zero potential B.C. (3) required a more distant boundary to produce similar results, and the required computing time was between that required for B.C. (1) and B.C. (2).

All of these boundary conditions are effected by treating a boundary point as an interior point, and by adding the appropriate "off-grid" potential. Equation (3-12) and (3-13) also require modification at exterior points since if the maximum (minimum) value of x in the model is X_{II} (X_I) the point X_{II+1} (X_0) does not exist. The required modifications for A_N, A_S, $(\partial\phi/\partial n)_E$ and $(\partial\phi/\partial n)_W$ are respectively:

$$A_N = \frac{1}{4}(x_{i+1} - x_{i-1})(z_{k+1} - z_{k-1}) + \frac{1}{2}(x_{II} - x_{II-1})(z_{k+1} - z_{k-1}), \text{ for } i = II;$$

$$A_S = \frac{1}{2}(x_2 - x_1)(z_{k+1} - z_{k-1}), \text{ for } i = 1;$$

$$\left(\frac{\partial \phi}{\partial n}\right)_E = \frac{\phi_E - \phi}{x_{i+1} - x_i} \leftrightarrow \frac{\phi^*_E - \phi}{-(x_{II-1} - x_{II})},$$

and

$$\left(\frac{\partial \phi}{\partial n}\right)_W = \frac{\phi_W - \phi}{x_i - x_{i-1}} = \frac{\phi^*_W - \phi}{(x_2 - x_1)}$$

where the asterisk indicates that ϕ^* is chosen subject to the boundary condition.

With the appropriate consideration of exterior points, we can now apply equation (3-13) to all grid points giving a system of linear equations that is solved by the method of over-relaxation (O.R.) (Stiefel, 1963). Faster and more sophisticated methods are discussed by Hockney (1965), but O.R. has been chosen for its programming simplicity and versitility. To derive the O.R. formula used in Panel's relaxation algorithm, we first cast the system of equations produced by equation (3-13) into the form

$$\sum_{m=1}^{M} C_{pm}\, \phi_m - Q_p = 0, \qquad p = 1, 2, \cdots\cdots M \tag{3-14}$$

where M is the total number of grid points. The solution of the p equation with respect to the central unknown ϕ_p yields:

$$\phi_p = \frac{1}{C_{pp}} \left[Q_p - \sum_{m \neq p} C_{pm}\, \phi_m\right] \tag{3-15}$$

This equality will not be satisfied until the problem has relaxed or converged to the final result. When (3-15) is not satisfied, we assume the righthand side to be the better value for ϕ_p, so by denoting the various approximations by the index υ we step through the index p, replacing ϕ_p^{υ} with $\phi_p^{\upsilon+1}$ to arrive

at the computational rule,

$$\phi_p^{\upsilon+1} = \frac{W}{C_{pp}} \left[Q_p - \sum_{m=1}^{p-1} C_{pm} \phi_m^{\upsilon+1} - \sum_{m=p+1}^{M} C_{pm} \phi_m^{\upsilon} \right]$$

We have jumped ahead and added the over-relaxation factor W. In the ordinary single step method, W = 1, and for W > 2 the method will diverge. The matrix C_{pm}, obtained from the discretization of a boundary value problem is of the banded symmetric-definite type, and for such, convergence is insured for W < 2; Panel uses W = 1.9 with no divergence problems.

In the program, the subroutine FIELD controls the Poisson calculation. The calculation of the interior coefficients is delegated to the subroutines CNS, CEW, and CUD. The boundary conditions and B.C. influenced coefficients are effected in FIELD and the subroutine RELAX performs the relaxation operation.

THE VLASOV PROBLEM

In kinetic theory, the density and current at a point $\vec{x}'$ are given by the 0th and 1st velocity moment of the single particle distribution function:

$$N_x(\vec{x}') = \int f_s'(\vec{x}', \vec{v}')\, d^3\vec{v}' \tag{3-16}$$

$$\vec{J}_s(\vec{x}') = q_s \int f_s'(\vec{x}', \vec{v}')\, \vec{v}' \cdot \hat{n}\, d^3\vec{v}', \tag{3-17}$$

where $\hat{n}$ is the unit vector in the direction of $\vec{J}_s'$. The distribution function is the density of particles in six-dimensional phase space (three position and three velocity coordinates). Further progress now requires finding ' at $\vec{x}'$.

Application of Liouville's theorem to a collisionless plasma leads the collisionless Boltzmann or Vlasov† equation (Montgomery and Tidman, 1964).

$$\frac{Df_s}{Dt} = \frac{\partial f_s}{\partial t} + \vec{v}\cdot\nabla f_s + \frac{q_s}{m_s}(\vec{E} + \vec{v}\times\vec{B})\cdot\nabla_v f_s = 0. \qquad (3\text{-}18)$$

In words, f_s is constant along a particle's path in six-dimensional phase space, which can be characterized by the constants of the motion. In a general electrostatic field such a constant is the total energy, defined by

$$H_s(\vec{x}, \vec{v}) = \frac{1}{2} m_s \vec{v}^2 + q_s V(\vec{x})$$

where $q_s V(\vec{x})$ is the potential energy of the particle at $\vec{x}$. The six-dimension phase space path projected onto the usual space coordinates is just the usual trajectory of a particle prescribed by Newtonian mechanics.

Consider the trajectory connecting $(\vec{x}', \vec{v}')$ with $(\vec{x}, \vec{v})$ for a given electrostatic field where at $\vec{x}$, the distribution of particles of specie s is known to be $f_s(\vec{x}, \vec{v})$. If f_s can be written as a function of only $H(\vec{x}, \vec{v})$, and since $H(\vec{x}', \vec{v}') = H(\vec{x}, \vec{v})$; we have therefore

$$f_s(H(\vec{x}, \vec{v})) = f_s'(H(\vec{x}', \vec{v}'));$$

---

†The Vlasov equation represents the zeroth order terms in a cluster expansion of the Liouville equation, with smallness parameter $g = (n_0\lambda_d^3)^{-1}$, the inverse of the number of particles in a Debye sphere. For GEO under substorm conditions n_e = 1/cc and kT_e = 10kev, $g = 10^{-9}$, so the collisionless approximation is a very good one. However, in the F region with $n = 10^6$/cc and kT_e = .2ev, g = 10 suggesting that the transport problem there needs a more detailed treatment.

or simply $$f'_s(\vec{x}', \vec{v}') = f_s(\vec{x}, \vec{v}). \tag{3-19}$$

We have now effectively solved the Vlasov equation and may now, in principle, proceed to evaluate the integrals in equations 3-16 and 3-17.

Note that some different value of $\vec{v}'$ will map to a different point $(\vec{x}_2, \vec{v}_2)$ where we know the distribution function to be different (or zero). Thus, in evaluating the integrals in equations (3-16) and (3-17), equation (3-19) must be used to develope a composite expression for f'. For example, consider the problem of a non-emitting body immersed in a Maxwellian plasma. At infinity, the distribution function in three-dimensions, for specie s is,

$$f_s(\vec{\infty}, \vec{v}) = N_s\left(\frac{m_s}{2\pi kT_s}\right)^{3/2} \exp\left[-\frac{H(\vec{v})}{kT_s}\right]. \tag{3-20}$$

At some point $\vec{x}'$ near the body, the distribution function will be,

$$f'_s(\vec{x}', \vec{v}') = N_s\left(\frac{m_s}{2\pi kT_s}\right)^{3/2} \exp\left[-\left(\tfrac{1}{2} m_s \vec{v}_s'^2 + q_s V(\vec{x}')\right)/kT_s\right] \times G_s(\vec{x}', \vec{v}'), \tag{3-21}$$

where G_s is a function with a value of either zero or one depending on whether $(\vec{x}', \vec{v}')$ maps to a non-source or source at infinity. In other formulations, the G function is effectively replaced by reconstructing the limits of integration in equations (3-16) and (3-17).

In practice, the integrals in (3-16) and (3-17) are approximated by summations over a discrete set of velocities where each value of $\vec{v}'$ represents a trajectory that must be followed to evaluate $G(\vec{x}', \vec{v}')$. We now have the choice of either starting trajectories at "infinity" and following them in; or because of the assumed time-independence, we could start at $\vec{x}'$ and follow trajectories backwards in time to "infinity". The first technique has been

dubbed the "Outside-in Method" by Parker (1964) and has the advantage of having all trajectories successfully connecting to a source and of supplying usefull trajectory information to all points along the trajectory. Its chief disadvantage lies in the difficulty of getting adequate trajectory probing of some regions of the problem. The Inside-out Method adopts the other approach of following trajectories backwards in time. This allows one to evaluate $G(\hat{x}', \hat{v}')$ at all points with equal accuracy, but can lead to large numbers of trajectories to be retraced with each iteration. This last difficulty has been recently overcome by recording the fate of each trajectory so that in subsequent iterations, that information can be used to trace only those trajectories that lie on the velocity space boundary between null and escaping trajectories. This "boundary tracking" innovation can greatly increase storage requirements, but the reduction in time requirements make it essential.

In the following paragraphs I shall described how PANEL performs the integrals (3-16) and (3-17). Parts of this description has been taken directly from Parker (1977).

It is convenient to transform (3-16) and (3-17) to energy and angle variables in velocity space. Since we will be primarily interested in Maxwellian energy distributions, we may adopt the following units in terms of which dimensionless variables may be defined:

kT = unit of energy, where T is the temperature of the Maxwellian distribution;

$\sqrt{2KT/m}$ = unit of velocity, namely, the most probably thermal velocity;

N_0 = unit of particle density, the unperturbed density;

$J_0 = \sqrt{kT/2\pi m}$ = unit of current, the undisturbed thermal current.

The energy and angle variables are:

H = energy in multiples of kT;

α = polar angle with respect to z-axis;

β = azimuthal angle with respect to the plane containing the z-axis and the point $\hat{x}$.

These angles which define the orientation of the velocity vector $\hat{v}$, are illustrated in figure 3/2. Note that the potential energy ϕ is also in units of kT, so with the new unit of velocity we can write: $H = v^2 + \phi$.

The density and current integrals (3-16) and (3-17) may be written

$$N_s = \iiint f' v^2 dv \sin\alpha \, d\alpha \, d\beta \, G$$

$$J_s = \iiint f' v^3 dv \cos\alpha \sin\alpha \, d\alpha \, d\beta \, G$$

where J_s is assumed to be the current to a surface perpendicular to the z-axis. Introducing now, the Maxwell distribution (without drift), we have

$$n = \frac{N_s}{N_0} = \frac{1}{2\pi^{3/2}} \int_{\max(0,\phi)}^{\infty} e^{-H} \sqrt{H - \phi} \, dH \int_0^{\pi} \sin\alpha \, d\alpha \int_0^{2\pi} G \, d\beta \qquad (3\text{-}22)$$

$$j = \frac{J_s}{J_0} = \frac{1}{\pi} \int_{\max(0,\phi)}^{\infty} e^{-H} (H - \phi) \, dH \int_0^{\pi/2} \cos\alpha \sin\alpha \, d\alpha \int_0^{2\pi} G \, d\beta \qquad (3\text{-}23)$$

The lower limit on the energy integral is chosen to be zero for an attractive potential ($\phi < 0$), and to be ϕ for a repulsive potential ($\phi > 0$). This ensures that we never consider particles with negative kinetic energy.

The integrals in (3-22) and (3-23) are evaluated by the method of Gaussian quadrature (Jennings, 1964). It is not feasable to derive it here, but the method can be illustrated by stating that in the formula

$$\int_a^b f(x) \, dx = \sum_{i=0}^{n} A_i f(x_i) + R$$

it is possible to choose A_i and x_i such that $R = 0$ for $f(x)$ any polynomial of degree $\leq 2n + 1$. When attempting to integrate a function of undetermined degree, it is desirable to make n as large as possible. This poses two problems: 1) the formulas for x_i and A_i get increasingly complicated as n increases and 2) the step function nature of $G(\vec{x}, \vec{v})$ implies a polynomial of infinite degree. Both problems are partially overcome by dividing the integration interval uniformly as for ordinary trapezoidal integration, and then applying a Gaussian quadrature of order 2 to each subinterval. Thus, in preparation for this, we transform the ranges of integration into intervals between -1 and +1 by the transformations:

$$H(c) = \frac{1 + c}{1 - c} + \max(0, \Phi), \qquad -1 < c < +1 \qquad (3\text{-}24)$$

$$\begin{aligned} \alpha &= \cos^{-1}\sqrt{(1 - a)/2} && \text{for current} \\ \alpha &= \cos^{-1}(-a) && \text{for density} \end{aligned} \qquad -1 < a < +1 \qquad (3\text{-}25)$$

$$\beta = \pi (1 + b), \qquad -1 < b < +1 \qquad (3\text{-}26)$$

The transformed current and density integrals then become,

$$n = \frac{1}{\sqrt{\pi}} \int_{-1}^{+1}\int_{-1}^{+1}\int_{-1}^{+1} e^{-H(c)} \sqrt{H(c) - \Phi}\, G \frac{da\, db\, dc}{(1 - c)^2} \qquad (3\text{-}27)$$

$$j = \frac{1}{2} \int_{-1}^{+1}\int_{-1}^{+1}\int_{-1}^{+1} e^{-H(c)} (H(c) - \Phi) \frac{G\, da\, db\, dc}{(1 - c)^2} \qquad (3\text{-}28)$$

We now have the integrals in a form suitable for Gaussian quadratures. We now divide the c-range into M_c sub-intervals, and apply a Gaussian quadrature of order 2 to each. Similarly, we divide the a-range and b-range into M_a and M_b sub-intervals, with Gaussian quadratures of order 2 applied to

each sub-interval. Now, both equations (3-27) and (3-28) can be put in the form

$$I = \int_{-1}^{+1}\int_{-1}^{+1}\int_{-1}^{+1} W(H)\cdot G(H, \alpha, \beta)\cdot da\ db\ dc \qquad (3\text{-}29)$$

which may be approximated by the sum:

$$I = \frac{1}{M_a M_b M_c} \sum_{K_c=1}^{M_c} \sum_{K_a=1}^{M_a} \sum_{K_b=1}^{M_b} \left[W(H^-)\cdot G(H^-, \alpha^-, \beta^-) + W(H^+)\cdot G(H^+, \alpha^+, \beta^+)\right] \qquad (3\text{-}30)$$

where W is the energy weight function defined by,

$$W(H) = \frac{e^{-H(c)}\,[H(c) - \phi]}{2(1 - c)^2} \qquad \text{for current}$$

$$W(H) = \frac{e^{-H(c)}\,\sqrt{H(c) - \phi}}{\sqrt{\pi}\,(1 - c)^2} \qquad \text{for density} \qquad (3\text{-}40)$$

with

$$H^- = H(c^-)\ ,\ H^+ = H(c^+)$$
$$\alpha^- = \alpha(a^-)\ ,\ \alpha^+ = \alpha(a^+)$$
$$\beta^- = \beta(b^-)\ ,\ \beta^+ = \beta(b^+).$$

Gaussian quadrature of order 2 applied to the interval -1, +1 yields the abscissas $\pm (3)^{-1/2}$ with a weight coefficient of unity. Applying this simple formula to each sub-interval gives the formula,

$$i^{\pm} = \frac{1}{M_i}\left[\pm \frac{1}{\sqrt{3}} + 2K_i - 1 + M_i\right] \quad \text{for } i = a, b, c. \qquad (3\text{-}41)$$

so, with these formulae for a, b, and c, we may use equations (3-24) through

(3-26) to choose sets of trajectories to be followed backwards in time to either source or non-source regions and thus approximate the integrals for density and current.

In the first iteration only a small set of the total $8M_cM_aM_b$ trajectories are used, and in following iterations the number is increased until the maximum number of trajectories is being followed. This is an economizing move that doesn't affect the accuracy of the calculation since in the beginning iterations, densities are only approximate. As each trajectory is followed to its end-point, its fate (escape = true, absorbed = false) is recorded in the four-dimensional logical matrix (N x $2M_c$ x $2M_a$ x $2M_b$) called TRYE for electrons and TRYI for ions, where N identifies the point. When each trajectory has been used at least once, the TRY matrices are used in subsequent iterations to trace only those that lie on a velocity space boundary. This is accomplished by simply comparing the last recorded fate for the trajectory in question to that for each of its six energy and angle neighbors in the TRY matrix. If all seven fates are identical, the trajectory is not followed and its fate is merely read from TRY. If they are not all identical, the trajectory is followed and any change of fate is recorded in TRY. If all the fates for a point and particle become the same, a shut-out would occur and no trajectories would be traced. To prevent this, all of the highest energy trajectories are exempted from the boundary searching process, and traced each iteration.

Trajectories

In an electrostatic field with no magnetic fields, a particle will move according to the equation,

$$\vec{x} = \vec{x}_0 + \vec{v}t + \frac{1}{2}\frac{q}{m}\vec{E}t^2$$

where t is time and $\vec{E}$ is the electric field. This equation is put into the units common to PANEL with the transformation $t \rightarrow t' \cdot (2kT/m)$. Thus we have

$$\begin{aligned} x &= x_0 + v_x t' + \tfrac{1}{2}\left(-\frac{1}{2}\frac{\partial \Phi}{\partial x}\right) t'^2 \\ y &= y_0 + v_y t' + \tfrac{1}{2}\left(-\frac{1}{2}\frac{\partial \Phi}{\partial x}\right) t'^2 \\ z &= z_0 + v_z t' + \tfrac{1}{2}\left(-\frac{1}{2}\frac{\partial \Phi}{\partial x}\right) t'^2 \end{aligned} \qquad (3\text{-}42)$$

where as before, v is in units of the most probable thermal velocity, and Φ is the dimensionless potential.

PANEL traces particle trajectories on the same grid that is used for the Poisson calculation. At each interior grid point, the six neighboring intermediate points each define a face of a cell enclosing the grid point. The velocities in equations (3-42) are always given as a result of a previous step, or as initial conditions as a trajectory starts. The partial derivatives of the potential in (3-42) are approximated by divided differences calculated in the following manner. At the point $P(x_i, y_j, z_k)$, form the west and east potential differences,

$$\Delta\Phi_W = \Phi(i, j, k) - \Phi(i-1, j, k)$$

$$\Delta\Phi_E = \Phi(i+1, j, k) - \Phi(i, j, k)$$

and similarly for y and z. Next, the absolute value $|(\Delta\Phi_W - \Delta\Phi_E)|$ is compared to the particle's total energy, H, multiplied by an input resolution factor RES. If the variation in potential differences is less than H • RES, PANEL uses

$$\frac{\Delta\Phi}{\Delta x} = \frac{\Delta\Phi_W + \Delta\Phi_E}{x_{i+1} - x_{i-1}},$$

for the entire cell, and if the variation is too great, the cell is halved and for the west and east halves we use,

$$\left(\frac{\Delta\Phi}{\Delta x}\right)_W = \frac{\Delta\Phi_W}{x_i - x_{i-1}}$$

and

$$\left(\frac{\Delta\Phi}{\Delta x}\right)_E = \frac{\Delta\Phi_E}{x_{i+1} - x_i}.$$

Thus, a cell can conceivably be divided into eight sub-cells. This subdivision is always performed at the start of a trajectory when the particle will probably never enter most of the sub-cells.

Once the cell or sub-cell has been defined and the "electric field" calculated equations (3-42) are solved independently for the times required to cross the cell, and the shortest positive time is chosen. Using this time, the particle is stepped to another face of the cell and the process begins again in the next cell until an outer boundary is reached. At a boundary, a particle can escape, be absorbed on a surface, or be reflected (for a reflection boundary condition).

STABILITY AND CONVERGENCE

Parker and Sullivan (1970) have analized the stability and convergence of the inside-out method, applied to a uniformly charged sphere in a uniform plasma. Although a three-dimension method like PANEL could be expected to differ from a simple one-dimension method in its stability properties, tests have shown that the results of their study are applicable to PANEL. That analysis will be briefly outlined.

If we imagine that the Poisson solving process can be represented by the operator $L(\Phi)$ and that the Vlasov process can be represented by $\vec{F}(\Phi)$, then the state of a system would be prescribed by

$$L(\Phi) = F(\Phi), \tag{3-43}$$

and the iterative procedure previously described would follow the Picard iteration rule,

$$L(\Phi_{n+1}) = F(\Phi_n), \tag{3-44}$$

where n is the iteration index. This iteration scheme, however, was found to diverge when the distance between their sphere and the model boundary exceeded the Debye length. An effective cure for this, is to replace rule (3-44) with

$$L(\Phi_{n+1}) = F(\alpha\Phi_n + (1 - \alpha)\,\Phi^M_{n-1}), \qquad 0 < \alpha < 1. \tag{3-45}$$

This technique is called mixing, and the superscript M indicates previously mixed potentials, i.e.,

$$\phi^M_{n-1} = \alpha\phi_{n-1} + (1 - \alpha)\phi^M_{n-2} .$$

Their analysis of rule (3-45) predicts monotone convergence for $\alpha < 2/(2 + y)$, oscillatory convergence for $2/(2 + y) < \alpha < 2/(1 + y)$, and divergence for $\alpha > 2/(1 + y)$, with an optimum value, $\alpha_{opt} = 2/(1 + y)$. The parameter y is given by

$$y = 2d^2/\pi^2\lambda_D{}^2,$$

where d is the boundary-object separation distance, and λ_D is the Debye length for the plasma. These predictions have been proven to be accurate for the one-dimension sphere model.

One could insure convergence by choosing α very small, but then a large number of iterations would be required. Therefore it is desireable to optimize α. With PANEL, I have found this prediction for α_{opt} to be a good first approximation; but to really obtain optimal convergence, calculations must be stopped every three or four iterations to adjust α.

4: RESULTS

The results presented here are of two distinct types: "calibration" models designed to test PANEL against problems for which analytic answers are available, and two production models to demonstrate PANEL's capabilities. Thus far, the emphasis has been on the former. Just as with an instrument, results are worthless without calibration. This emphasis has been rewarded, as many subtle errors (both with PANEL and my use of PANEL) have been detected and corrected. For this reason, the runs presented here represent only a fraction of those that have been made.

The models called Gap 06, Gap 07, and Gap 08 are calibration models of the problems described in equations (2-12) through (2-17) in section 2 of this report. Pan 21 is a model of a planar electron diode, and can be compared to the Child-Langmuir law, equation (2-20). Finally, Pan 29 and Pan 36 are production models of charged panel in a plasma similar to that encountered in the Chamber A experiments at the Johnson Space Center (McCoy and Konradi, 1978). All of these are two-dimensional models. Three-dimensional tests have also been made, but limited computing time has prevented the running of physically meaningful three-dimensional models.

In the gap problem, electrons are accelerated from a cold cathode ($T = 0$) to the potential V_1 (see figure 2/1) at $x = 0$, to produce a beam current J. PANEL models this experiment by assuming that there is an undisturbed Maxwellian plasma at $x_1 < -d$, so that the current J is the random thermal current ($J_0 = N_0 e \sqrt{kT/2\pi m}$) crossing the grid at $x = -d$. (Although the plasma has density N_0, the electrons crossing the grid have $N = N_0/2$). As described in section 2, this current is normalized by the relevent C-L current, thus we have the current ratio,

$$\beta = J/J_{CL}.$$

The results of Gap 06, Gap 07, and Gap 08 are plotted in figures 4/1 and 4/2. In these plots, the transmitted electrons travel from right to left across a gap of one meter. This is modeled by 24 grid points; 12 z and 2 x coordinates. At z = 0 electrons are absorbed; at z = 11 (not shown), they are generated; and they are reflected at both x boundaries. (Since this is a one-dimension problem, PANEL could have been fitted with a one-dimension option, but unlike the two-dimension option, a one-dimension option would have only limited applications.) In all three plots, the potentials predicted by the classical theory are labeled as curve A, and the results of PANEL are labeled P. The features of these models are:

Gap 06: $\beta = 10$, $J = 2.373 \times 10^{-2}$ A/m^2, $T_e = 10$ eV, $V_1 = 100$ V, $N_0 = 2.8 \times 10^5$ cm^{-3}, $M_e = 4$, $M_a = 32$;

Gap 07: $\beta = 10$, $J = 2.373 \times 10^{-2}$ A/m^2, $T_e = 1$ eV, $V_1 = 100$ V, $N_0 = 8.9 \times 10^5$ cm^{-3}, $M_e = 4$, $M_a = 32$;

Gap 08: $\beta = 4$, $J = 9.49 \times 10^{-3}$ A/m^2, $T_e = 1$ eV, $V_1 = 100$ V, $N_0 = 3.5 \times 10^5$ cm^{-3}, $M_e = 4$, $M_a = 32$.

Gap 07 and 08 are both well converged, but Gap 07 has an uncertainty indicated by the error bar on the plot. I consider these models to be a positive test of PANEL, inspite of the large deviations from the classical predictions. The classical theory considers a source of electrons with no thermal spread. By comparing Gap 06 with Gap 07 we can see that as the source plasma cools from a temperature of 10 eV to 1 eV, the results get closer to the classical predic-

tion. In Gap 08 where $\beta = 4$, the predicted minimum potential is 75.0 volts while PANEL gives 75.1 $\pm$ 0.7 (the error indicates the degree of convergence). This again indicates that the disagreement with the classical theory in Gap 06 and Gap 07 are due to non-zero temperatures since one would expect this effect to be most pronounced with low minimum potentials, and least pronounced with higher minimum potentials.

From Gap 08 we can also learn something about the number of trajectories that must be traced to give accurate densities. In figure 4/2, the lower curves labeled D and C are densities for PANEL and classical theories respectively. Briefly, the classical densities are derived by eliminating v from

$$J = Nev \tag{4-1}$$

and

$$\frac{1}{2} mv^2 = eV \tag{4-2}$$

to get

$$N = J(m_e/2e^3 V)^{1/2}. \tag{4-3}$$

For Gap 08 the total zenith angle range of 2π is covered by 64 trajectories to give a trajectory separation of .098 rad. or 5.63°. This separation was further reduced by one half by noting that due to symmetry, positive and negative angles of equal magnitude lead to equivalent trajectories; thus all trajectories were shifted by half of the separation angle. The result is that although the voltages were obtained with good accuracy, the densities still lack resolution.

Pan 21 represents a simple but important test of PANEL. This is a comparison of PANEL with the Child-Langmuir law shown in fig. 4/3. Due to the close agreement, a curve has been drawn only through the PANEL points. At

selected points, PANEL and C-L potentials are given for comparison. The C-L potentials are given in parentheses and C-L densities are plotted with crosses. Here 32 points (2 x 16) were used to model a diode with a 16.51 meter plate separation, and a 100 volt potential difference. The model parameters are:

Pan 21; T_e = 1 eV, N = 3.2×10^2 cm^{-3}, λ_d = 0.4m, M_e = 4, M_a = 32,

J= 8.58×10^{-6} A/m^2

The greatest disagreement between PAN 21 and the C-L theory occurs at z = 14, whete the PANEL prediction is 22% high, with improved agreement at lower z values. At z = 8, the disagreement is only 1%. The larger deviations should be expected in the low voltage region near the cathode due to the non-zero injection velocity of the electrons. For this reason, it would be desireable to compare PANEL predictions with the modified C-L law, equation (2-10), but unfortunately, this comparison has not yet been made.

Pan 29 and Pan 36 are two-dimensional models of a cross-section of an infinitely long, one meter wide panel held at a potential of 100 volts in a hydrogen plasma with equal ion and electron temperatures of 10 eV. The chosen plasma temperature of 10 eV is higher than the usual temperatures encountered in LEO or in the JSC Chamber A experiments which are frequently less than 1 eV. Models with a panel potential of 100 V and a temperature of 1 eV have been considered, but under these conditions PANEL is significantly less stable. To achieve stability thus requires a smaller mixing parameter, more iterations and more computing time; so for these first models, a higher but not unreasonable temperature was chosen.

Due to the symmetry of the problem, it was possible to model the entire

cross-section by calculating potentials and densities in one quadrant only by using the reflection boundary condition on the DOWN and WEST boundaries. For PAN 29 the UP B.C. is V = 0, and for the EAST boundary the B.C. is the zero normal gradient boundary condition [B.C. (2), $\partial V/\partial n = 0$]. Model parameters for PAN 29 and PAN 36 are:

$$T_i = 10 \text{ eV}, \; T_e = 10 \text{ eV}, \; N_0 = 1.9 \times 10^4 \text{ cm}^{-3}, \; \lambda_0 = .17\text{m},$$
$$J_{oe} = 1.61 \times 10^{-3} \text{ A/m}^2, \; ME = 4, \; MA = 32.$$

PAN 29 potential contours are displayed in Figures 4/4, and the PAN 36 results are displayed in Figures 4/5, 4/6 and 4/7. The potential contours shown in Figures 4/4 and 4/5 were produced by the well-known technique of eyeball interpolation. For PAN 36, potentials (labeled P) and charge densities (labeled C) along the DOWN and WEST boundaries are presented in Figures 4/6a and b respectively, and the electron and proton densities along these same boundaries are shown in Figure 4/7. In addition to the change in B.C.'s the other differences between PAN 29 and PAN 36 are location of the boundaries and the number of grid points. PAN 29 has an UP boundary distance of 1.85 meters with a 8 x 8 grid, while PAN 36 has an UP boundary distance of 2.4 meters with a 9 x 10 grid.

Several interesting features of the general problem can be observed by comparing the contour plots 4/4 and 4/5. First, by assuming that PAN 36 is the better model of the two, we can see that B.C. (2) on the EAST boundary of PAN 29 (Figure 4/4) produced potentials along the DOWN boundary that are very close to those of PAN 36; and therefore supposedly better than what could have been obtained with a V = 0 condition. The drawback is that B.C. (2) severely destabilizes the problem. One model, PAN 35 (nearly identical to PAN 36, but

with B.C. (2) on both the UP and EAST boundaries) diverged severely with a mixing factor of 0.08, while PAN 36 was stable with mixing factors up to 0.5. This suggests the possibility of speeding convergence on smaller grids by using varying mixing factors with small values near B.C. (2) boundaries and increasing to larger values near fixed potentials.

It can also be seen that the increased grid point density near the panel in PAN 36 has caused the 70 V, 50 V, and 30 V contours to move closer to the panel with smoother contours near the edge of the panel. The electron currents collected from above the panel are indicated by the arrows below the panel in figures 4/4 and 4/5, and have been normalized by the random thermal current, J_0. Near the center of the panel, both models give the same current, but with the increased point density in PAN 36 we begin to see a slight reduction in current collection near the edge. A further increase in point density would probably show more current focusing. However, the strong central focusing (greater than an order of magnitude difference between central and edge currents) observed by McCoy (1980) in the solar panel tests at JSC is not indicated in these models. This focusing could be dependent on the correct choice of panel voltage and plasma parameters, but is most likely due to a band of dielectric along the edges of that test panel. This possibility will be tested in future models.

For both PAN 29 and PAN 36, the C-L screening distance is D_{CL} = 1.2 m, and the corrected screening distance is D_s = 1.73 m. These points are indicated in Figures 4/4, 4/5, 4/6, and 4/7, and the uncorrected C-L contour is marked with crosses in Figure 4/6. Figures 4/5 and 4/7 show that potentials have been reduced to less than kT/e (= 10 V) within either estimate. There is some "compression" of the contours caused by the closeness of the V = 0 boundaries, as is evidenced by the most distant points in Figure 4/7

where the electron density unrealistically drops below the proton density due to the artificially high electric field between the outermost two points. However, comparison of the EAST boundaries of Figures 4/4 and 4/5 suggests that this compression is not too severe.

Although all of the PAN 29 and PAN 36 boundaries are too close to allow an undisturbed plasma region to develop, Figure 4/7b shows a definite pre-sheath region beyond the D_{CL} point with electron and proton densities nearly equal but reduced from the ambient values.

The Models PAN 29 and PAN 36 are clearly not a complete study of the solar panel-plasma interaction problem, but the results that have been presented should demonstrate that PANEL is capable of accurate space charge calculations. Three-dimensional test calculations have been successfully run, but time limitations have prevented full scale three-dimensional modeling. The two-dimensional model PAN 29 required twelve minutes of processing on an ITEL AS/6. PAN 36 required about thirty minutes, and three-dimensional models are expected to require many hours of processing time. Although this is not an extreme requirement, two-dimensional modeling will continue to be important for deciding matters such as the placement of boundaries, or the effect of chamber walls.

Appendix A: Symbols and Constants

The symbols and constants used throughout this report are reviewed in this appendix. With only a few noted exceptions, the MKS system of units has been adhered to.

T; temperature in degrees Kelvin.

k; Boltzman's constant = 8.62×10^{-5} eV/°K.

e; electon charge = 1.602×10^{-19} Coulomb.

m_e; electron mass = 9.11×10^{-31} kilograms.

m_p; proton mass = 1.673×10^{-27} grams.

ε_0; free space permittivity = 8.85×10^{-12} farad/meter.

V; potential in Volts.

Φ; dimensionless potential normalized by kT/e.

v; velocity in meters/second, or normalized by $\sqrt{2kT/m}$.

E; dimensionless electric field.

H; total energy in Joules, or dimensionless total energy normalized by kT/e.

N; density in m^{-3}.

N_0; ambient density in m^{-3}.

n; dimensionless density normalized by N_0.

J; current in Amperes/meters^2 = Am^{-2}.

J_0; random thermal current in Am^{-2}.

j; dimensionless current normalized by J_0.

ρ; charge density in Coulomb m^{-3}.

a; sheath thickness.

λ_D; Debye length.

Appendix B: Subroutine linkage.

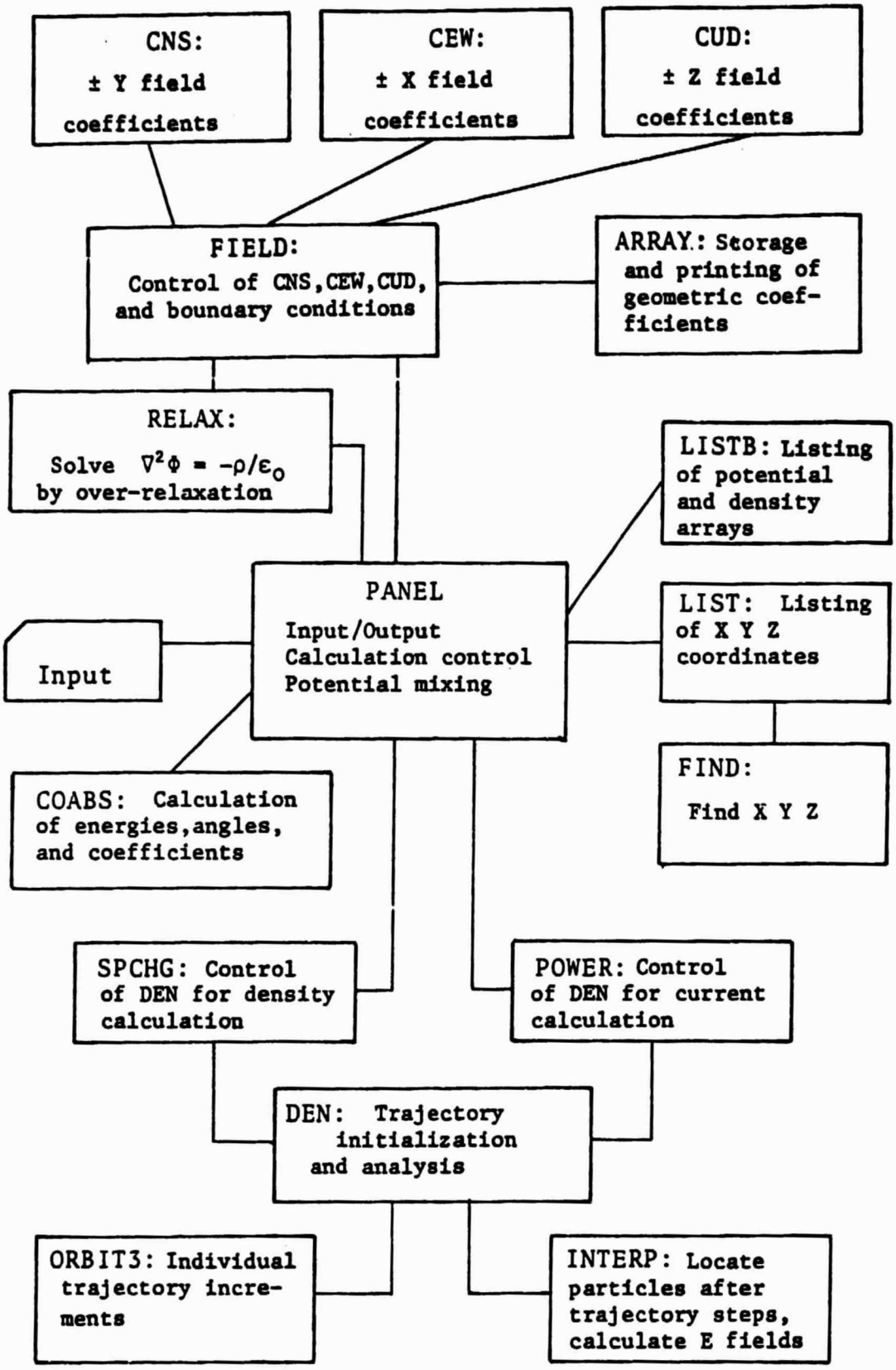

Appendix C: The 2-D Option

When a problem exhibits sufficient symmetry, it is sometimes possible to reduce the number of integrals in equations (3.16) and (3.17) that must be performed numerically; so, in a sense, PANEL's 2-D option still produces 3-D results.

Using the Maxwellian distribution given in (3.21), and writing (3.16) and (3.17) in terms of Cartesian velocity coordinates we have,

$$N(x') = N_o \left(\frac{m}{2\pi kT}\right)^{3/2} \int_{-\infty}^{\infty} dv_x' \int_{-\infty}^{\infty} dv_y' \int_{-\infty}^{\infty} dv_z' \; G(x', v') \qquad \text{(C-1)}$$

$$\times \exp\left[-\frac{m}{2kT}\left(v_x'^2 + v_y'^2 + v_z'^2\right) - \frac{q\,v(x')}{kT}\right]$$

$$\vec{J}(x') = q\, N_o \left(\frac{m}{2\pi kT}\right)^{3/2} \int_{-\infty}^{\infty} dv_x' \int_{-\infty}^{\infty} dv_y' \int_{-\infty}^{\infty} dv_z' \; G(x', v') \qquad \text{(C-2)}$$

$$\times (\vec{V} \cdot \hat{n}) \exp\left[-\frac{m}{2kT}\left(v_x'^2 + v_y'^2 + v_z'^2\right) - \frac{qV(x')}{kT}\right]$$

If $G(x', v')$ is not a function of v_y, and if $\hat{n}$ in (C-2) lies entirely in the x-z plane, the v_y integrations can be performed immediately leaving

$$N(x') = N_o \left(\frac{m}{2\pi kT}\right) \int_{-\infty}^{\infty} dv_x \int_{-\infty}^{\infty} dv_z \; G(x', v') \qquad \text{(C-3)}$$

$$\times \exp\left[-\frac{m}{2kT}\left(v_x'^2 + v_z'^2\right) - \frac{qV(x')}{kT}\right]$$

and

$$J_z(x') = N_o \left(\frac{m}{2\pi kT}\right) \int_{-\infty}^{+\infty} dv_x' \int_{o}^{\infty} dv_z' \; G(\vec{x}', \vec{v}')\, V_z \qquad \text{(C-4)}$$

$$\exp\left[-\frac{m}{2kT}\left(v_x'^2 + v_z'^2\right) - \frac{qV(x')}{kT}\right]$$

where we have set $\hat{n} = \hat{z}$. Transforming now to cylindrical polar coordinates, and as in Section 3, denoting the exponential argument by H; we have

$$N(x') = N_0\left(\frac{m}{2\pi kT}\right) \int_0^{\infty} v'dv' \int_{-\pi}^{+\pi} d\theta'\ G(\vec{x}', \vec{v}')\ \exp\ (-H) \qquad \text{(C-5)}$$

and

$$J_z = N_0\ \left(\frac{m}{2\pi kT}\right) \int_0^{\infty} v'^2 dv' \int_{-\pi/2}^{+\pi/2} \cos\ \theta'\ d\theta'\ G(\vec{x}', \vec{v}')\ \exp\ (-H) \qquad \text{(C-6)}$$

Again as in Section 3, we transform to dimensionless v, H, and Φ, and normalize by N_{so} and J_{so} to get the two-dimensional versions of (3-22) and (3-23);

$$n = \frac{1}{2\pi} \int_{\max(0,\Phi)}^{\infty} e^{-H}\, dH \int_{-\pi}^{+\pi} d\theta\ G(\vec{x}', \vec{v}') \qquad \text{(C-7)}$$

and

$$j_z = \frac{1}{\sqrt{\pi}} \int_{\max(0,\Phi)}^{\infty} e^{-H} \sqrt{H - \Phi}\ dH \int_{-\pi/2}^{+\pi/2} \cos\theta\ d\theta\ G(\vec{x}', \vec{v}') \qquad \text{(C-8)}$$

In preparation for Gaussian quadrature, we make the following transformatins:

$$E = \frac{1 + c}{1 - c} + \max(0,\Phi), \qquad -1 < c < +1 \qquad \text{(C-9)}$$

$$\begin{aligned} \theta &= \pi a && \text{,for density} \\ \theta &= \sin^{-1}(a) && \text{,for current} \end{aligned} \qquad -1 < a < +1 \qquad \text{(C-10)}$$

Including these we have,

$$n = \int_{-1}^{+1} \int_{-1}^{+1} e^{-H(c)}\, \frac{dc\ da}{(1 - c)^2}\, G(\vec{x}', \vec{v}') \qquad \text{(C-11)}$$

and

$$j_z = \frac{2}{\sqrt{\pi}} \int_{-1}^{+1} \int_{-1}^{+1} e^{-H(c)} \sqrt{H - \Phi}\, \frac{dc\ da}{(1 - c)^2}\, G(\vec{x}', \vec{v}')$$

And, as in section (3), we introduce the sub-interval Gaussian quadrature

approximations:

$$n \text{ or } j_z = \frac{1}{M_c M_a} \sum_{K_c=1}^{M_c} \sum_{K_a=1}^{M_a} [W_2(H^-)\cdot G_2(H^-,\theta^-) + W_2(H^+)\cdot G_2(H^+,\theta^+) \qquad \text{(C-12)}$$

where the two-dimensional energy weight function is

$$W_2 = \frac{e^{-H(c)}}{(1-c)^2} \times \begin{cases} 1 & \text{,for density} \\ \frac{2}{\sqrt{\pi}} \sqrt{H - \Phi} & \text{,for current} \end{cases} \qquad \text{(C-13)}$$

and $$H^{\pm} = H(c^{\pm}),\ \theta^{\pm} = \theta(a^{\pm}).$$

The Gaussian abscissa formula (3-41) and the transformations (C-9) and (C-10) are used to initiate trajectories.

REFERENCES

Birdsall, C. K., and W. B. Bridges, Electron Dynamics of Diode Regions, Academic Press, New York, N. Y., 1966.

Child, C. D., "Discharge from hot CaO," Phys. Rev., 32, 492, 1911.

Collatz, L., The Numerical Treatment of Differential Equations, Springer-Verlag, 1960.

Fay, C. E., A. L., Samuel, and W. Shockley, "On the theory of space charge between parallel plane electrodes," Bell Sys. Tech. J., 17, 1938.

Gill, E. W. B., "A space charge effect," Phil. Mag., 49, 993, 1925.

Hanley, G. M., "Satellite power systems (SPS) concept definition study," final report for NASA Contract NAS8-32475, Rockwell Int. Report #5078-AP-0023, Cincinnati, 1978.

Hockney, R. W., "Solution of Poisson's equation using Fourier Analysis," J. Assoc. Computing Mach., 12, 95, 1965.

Jackson, J. D., Classical Electrodynamics, Wiley and Sons, Inc., p. 341, 1962.

Jennings, W., First Course in Numerical Methods, MacMillan Co., New York, p. 129, 1964.

Langmuir, I., "The effect of space charge and residual gases on thermionic currents in high vacuum," Phys. Rev., 2, 450, 1913.

Langmuir, I., "The interaction of electron and positive ion space charges in cathode sheaths," Phys. Rev., 33, 954, 1929.

Langmuir, I., and K. B. Blodgett, "Currents limited by space charge between concentric spheres," Phys. Rev., 24, 49, 1924.

McCoy, J. E., and A. Konradi, "Sheath effects observed on a 10 meter high voltage panel in simulated low earth orbit plasma," Spacecraft Charging Technology--1978, ed. by R. C. Finke and C. P. Pike, AFGL-TR-79-0082, p. 315, 1978.

McCoy, J. E., "High voltage space plasma interactions," in Proceedings of the Solar Power Satellite Program Review, DOE/NASA, avail. from NTIS, 5285 Port Royal Road, Springfield, Virginia 22161, 1980.

Montgomery, D. C., and D. A. Tidman, Plasma Kinetic Theory, p. 51, McGraw-Hill, 1964.

Parker, L. W., "Numerical Methods for Computing the Density of a Rarefied Gas about a Moving Object," AFGL-64-193, Allied Res. Assoc., Inc., Concord, Mass., 1964.

Parker, L. W., "Computation of collisionless steady-state plasma flow past a charged disk," NASA CR-144159, Lee W. Parker, Inc., Concord, Mass., 1976.

Parker, L. W., "Calculation of sheath and wake stsructure about a pill-box shaped spacecraft in a flowing plasma," in Proceedings of the Spacecraft Charging Technology Conference, ed. by C. P. Pike and R. R. Lovell, AFGL-TR-77-0051, 331, 1977a.

Parker, L. W., Power loss calculation for high-voltage solar arrays, final report for NASA Contract NAS3-2085, Lee W. Parker, Inc. Report, 1977b.

Parker, L. W., "Plasma-photosheath theory for large high-voltage structures," in Space Systems and Their Interactions with the Earth's Space Environment, ed. by H. B. Garrett and C. P. Pike; Progress in Astronautics and Aeronautics, 71, American Inst. of Aeronautics and Astronautics, 1980.

Parker, L. W., and E. C. Sullivan, "Boundary conditions and iterative procedures for plasma sheath problems," in Sixth Int'l Symposium on Rarefied Gas Dynamics, II, 1969.

Parker, L. W., and E. C. Sullivan, "Numerical solution of the Poisson-Vlasov system for a spherical electrostatic probe," presented at S. I. A. M. Fall meeting, 1970.

Parker, L. W., and E. C. Whipple, "Theory of spacecraft sheath structure, potential, and velocity effects on ion measurements by traps and mass spectrometers," J. Geophys. Res., 75, 4720, 1970.

Reiff, P. H., J. W. Freeman, and D. L. Cooke, "Environmental protection of the solar power satellite," in Space systems and Their Interactions with Earth's Space Environment, ed. by H. B. Garrett and C. P. Pike; Progress in Astronautics and Aeronautics, 71; by Am. Inst. of Aeronautics and Astronautics, 1980.

Salzburg, B., and A. V. Haeff, "Effects of space charge in the grid-anode region of vacuum tubes," R. C. A. Rev., 2, 336, 1938: reprinted in Electron Tubes, 1935-1941, pub. by R. C. A. Rev., Princeton, N. J., 1949.

Stiefel, E. L., An Introduction to Numerical Mathematics, Academic Press, p. 199, 1963.

Whipple, E. C., "Modeling of spacecraft charging," Proceedings of the Spacecraft Charging Technology Conference, ed. by C. P. Pike and R. R. Lovell, AFGL-TR-77-0051, p. 225, 1977.

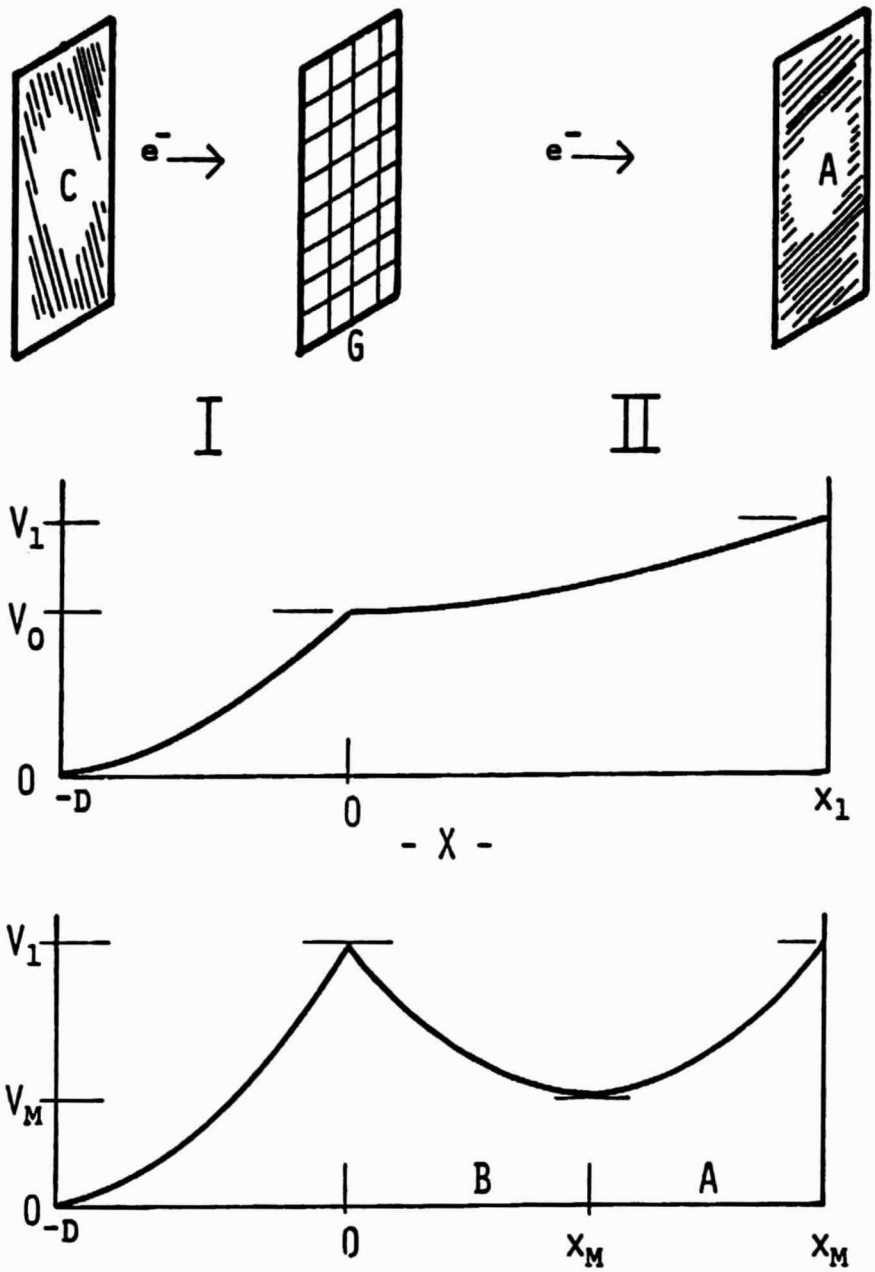

FIG. 2/1

Schematic representation of a planar electron diode, showing the effect of the electron space charge on the interelectrode potential for two different arrangements of the electrode potentials.

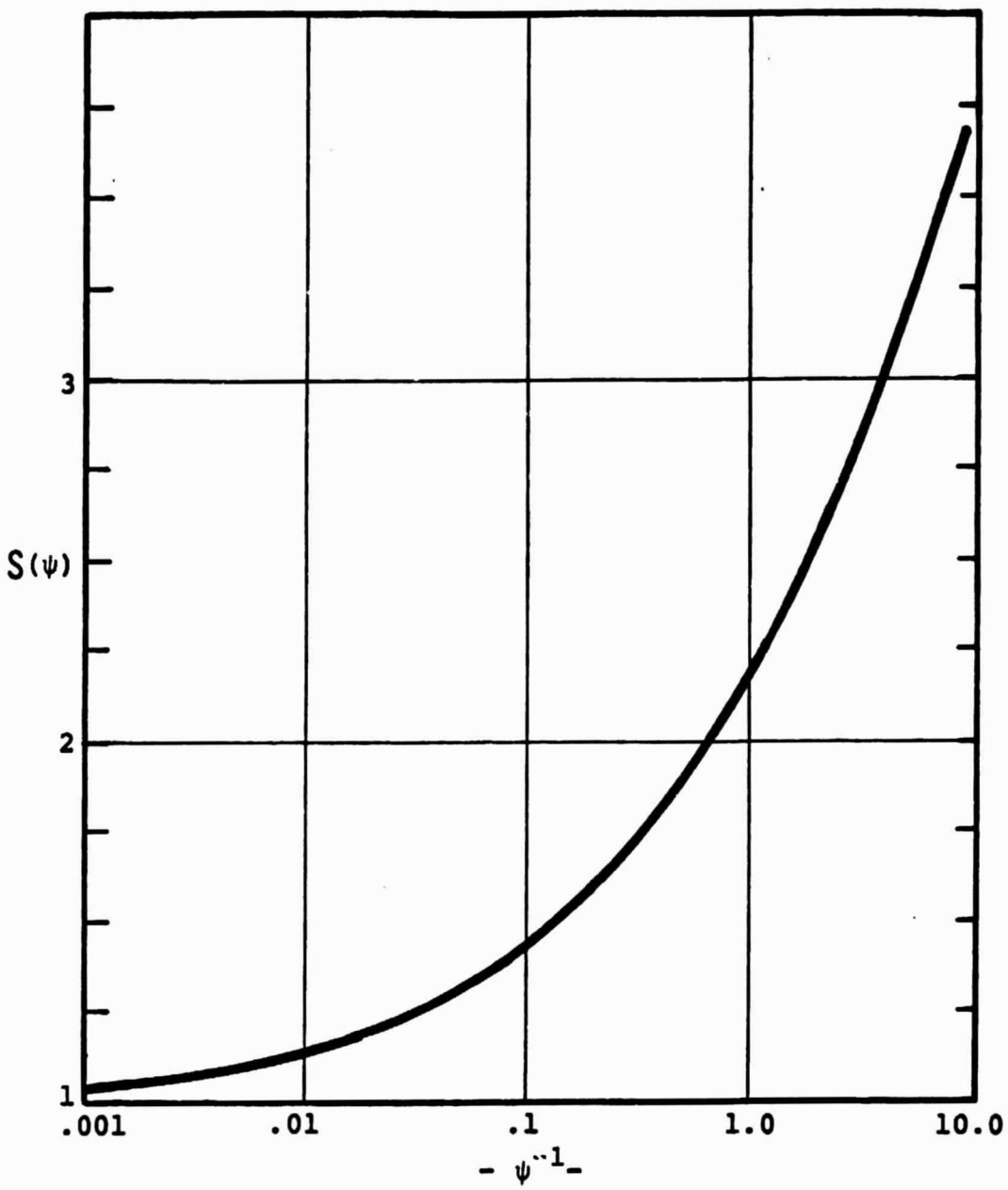

FIG.2/2. The Child-Langmuir correction function $S(\psi)$ plotted against $\log(\psi^{-1})$, where $\psi = V/kT$.

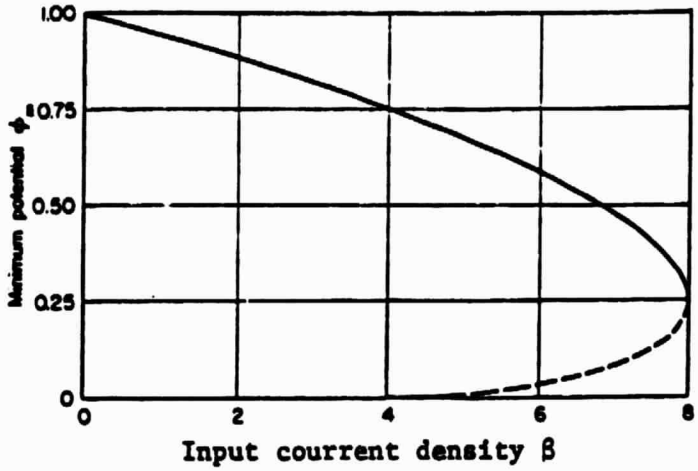

Fig.2/3a. Minimum potential ϕ_m as a function of input current β. The dotted portion is called the "C-overlap" solution and is excluded by stability considerations.

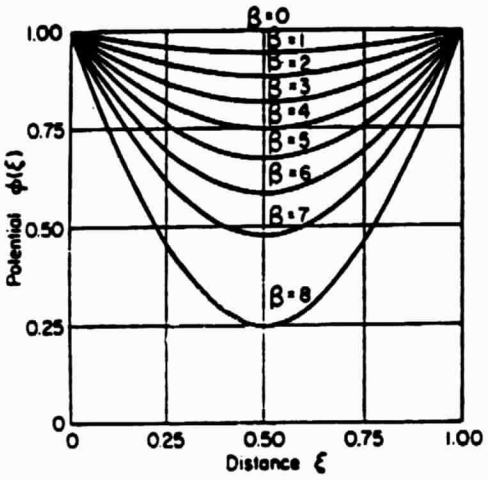

Fig.2/3b. Potential profiles in the interelectrode space for the classical,positive potential-minimum solutions with input currents between 0 and 8 .

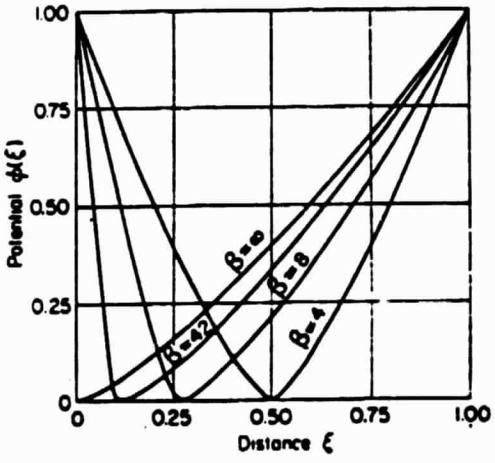

Fig.2/3c. Potential profiles in the interelectrode space for the classical virtual-cathode solutions ($\phi_m = 0$) with input currents between 4 and ∞ .

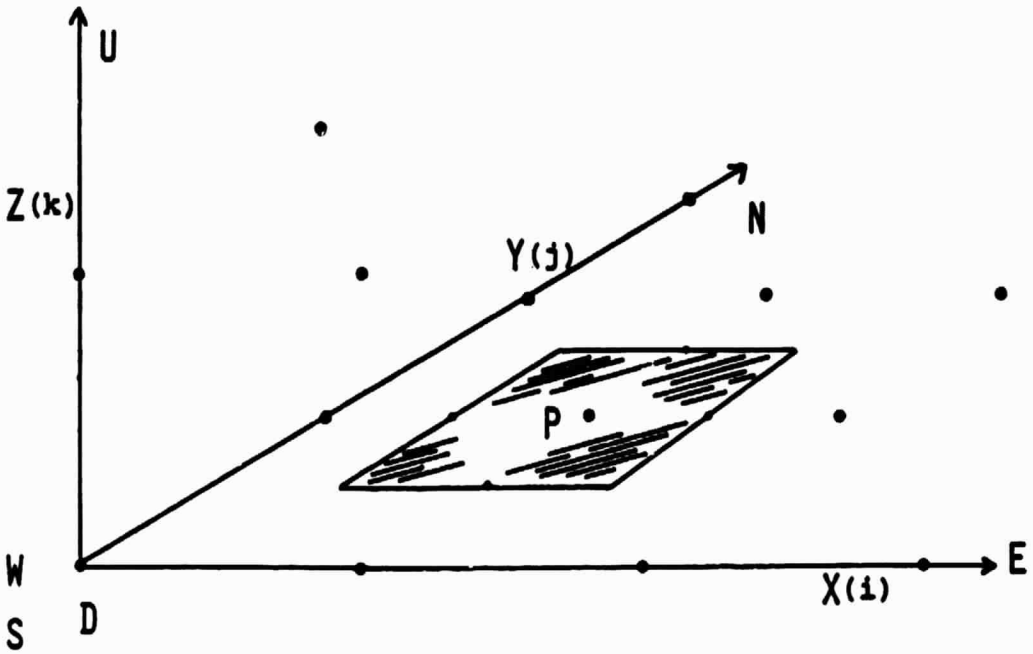

FIG.3/1. A sample grid illustrating a projection onto the X-Y plane of the volume associated with the point P, and the directions indicated by N,S, E,W,U, and D.

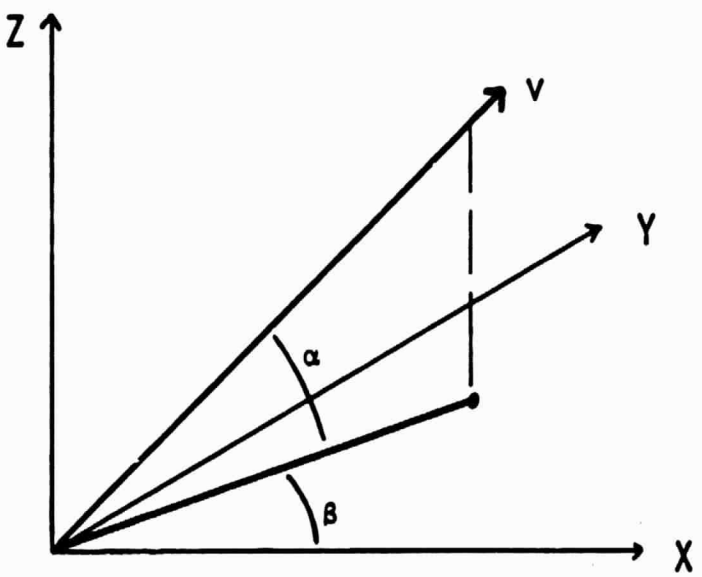

FIG.3/2. An illustration of the polar-spherical angles α and β used in PANEL.

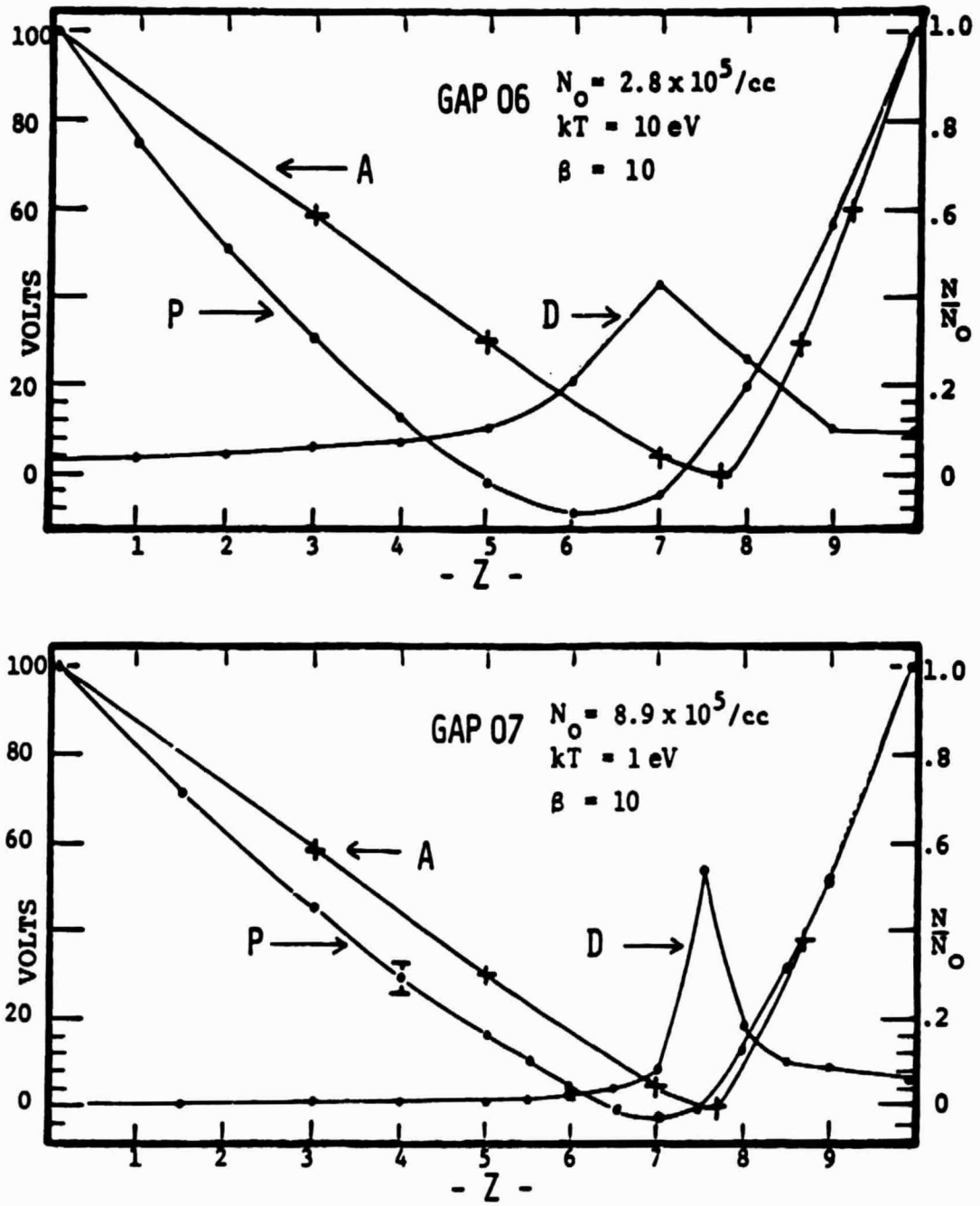

FIG.4/1: In both graphs, curve P is PANEL's prediction for the inter-electrode potentials, curve A is the classical prediction, and curve D is PANEL's prediction for the electron density. The Z distance unit is 0.1 meter. β is the normalized current density.

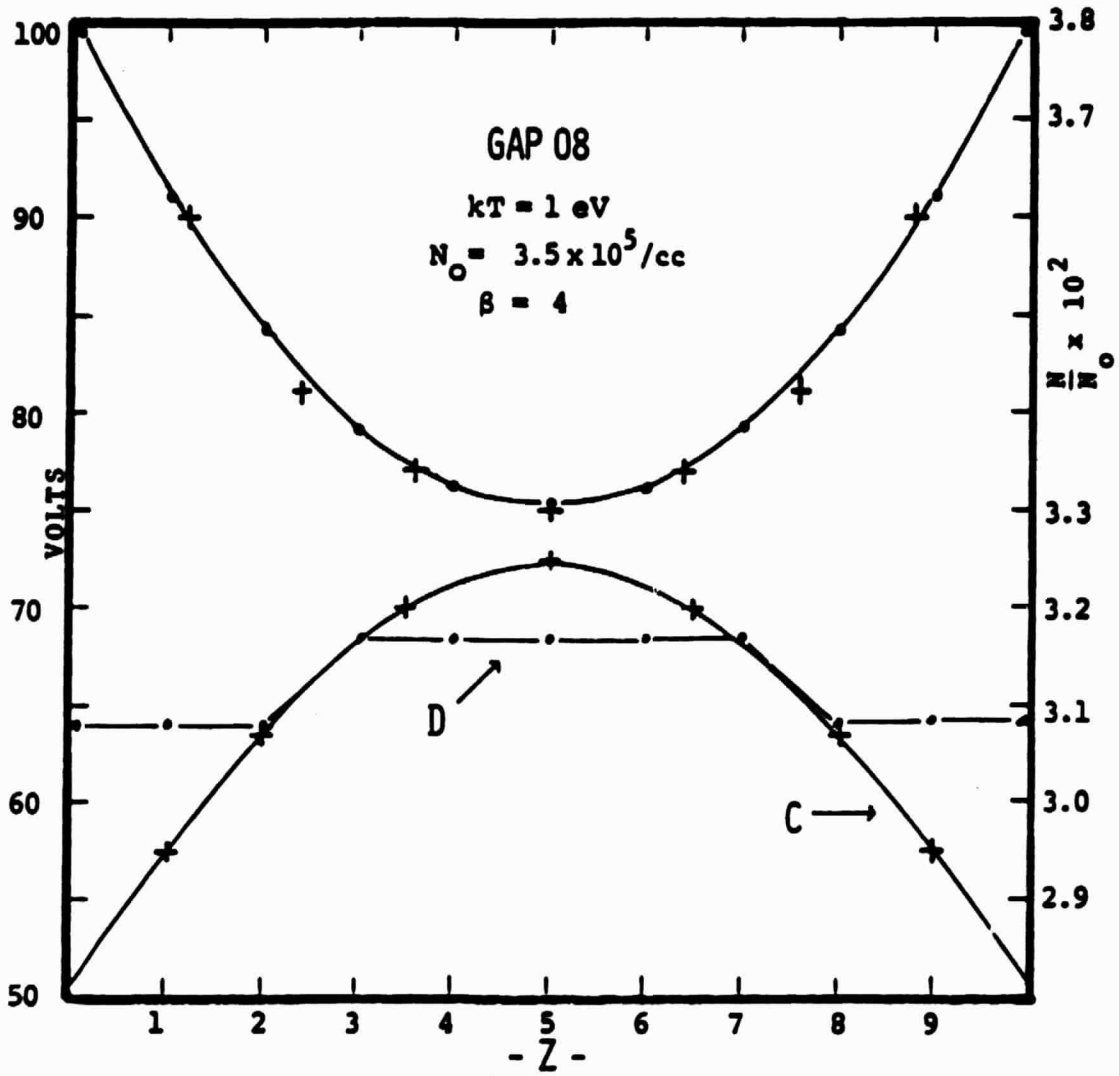

FIG.4/2: The upper curve is PANEL's prediction for the inter-electrode potentials, and the classical potentials are the unconnected crosses. Of the lower curves, D is the PANEL result for the densities, and C gives the classical densities. The Z unit of distance is 0.1 meter, and β is the normalized current density.

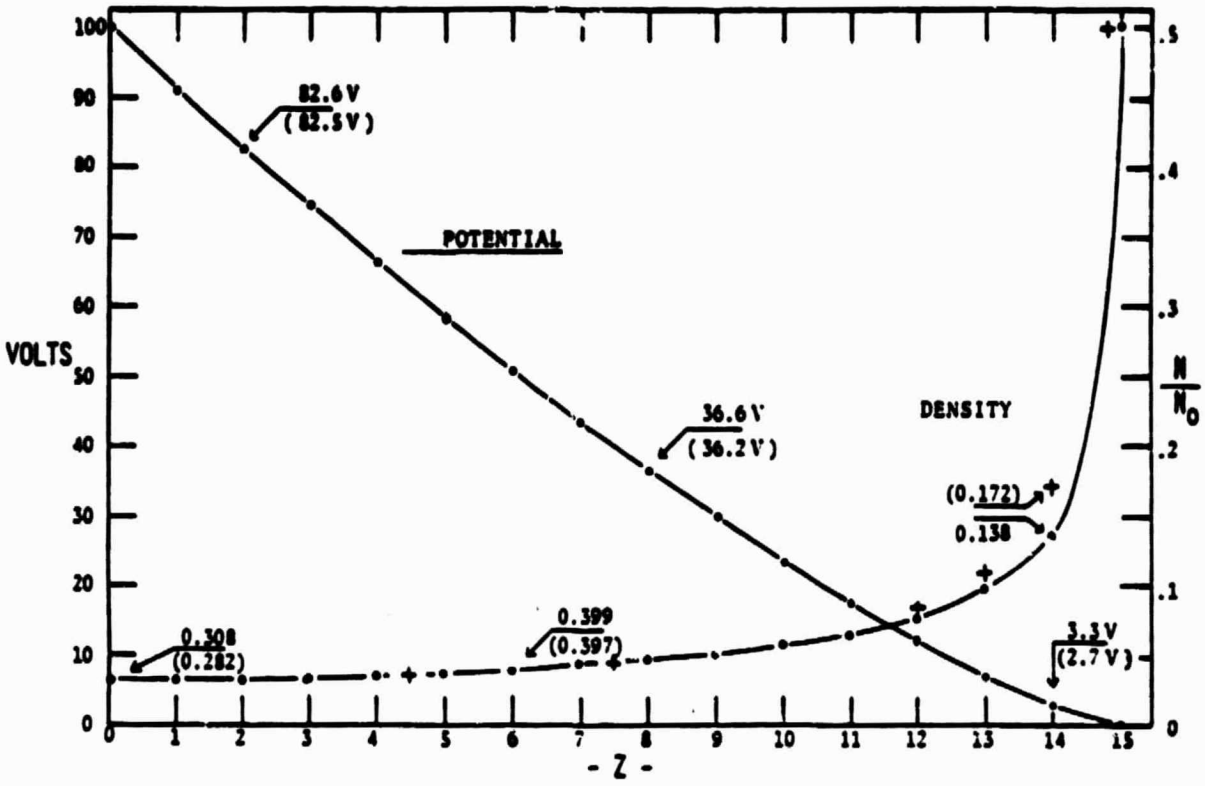

FIG.4/3: PANEL's predictions for the Child-Langmuir electron diode are plotted with the connected dots, and selected values of potential and density are presented. The classical C-L density predictions are plotted by the unconnected crosses, and for comparison, selected values of the C-L potential and density are given in parenthesis. For this model, $N_0 = 320/cc$, $J_e = 8.6 \times 10^{-6}\ A/m^2$, and the total diode separation is 16.51 meter.

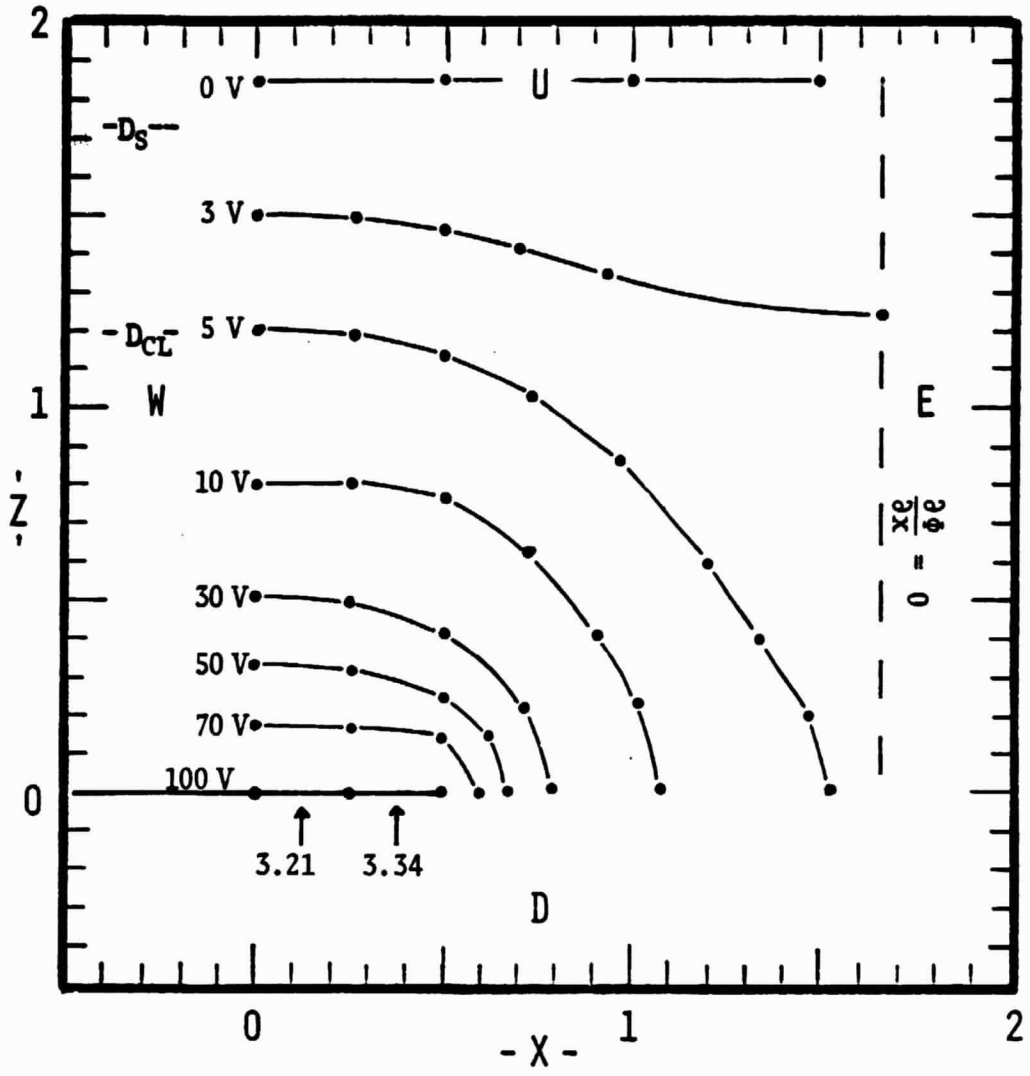

FIG. 4/4,Model Pan29: Equipotential contours about a 1 m wide, infinitely long panel, uniformly charged to 100 V; modeled with 64 grid points (not shown). The plasma temperature and density are kT = 10 eV, $N_o = 1.9 \times 10^4$/cc. The thermal currents are $J_{oe} = 1.61 \times 10^{-3} A/m^2$ for electrons, and $J_{op} = 3.76 \times 10^{-5} A/m^2$ for protons. The electron currents collected by the panel are indicated by the arrows below the panel and are normalized to J_{oe}; the average proton current to the panel is $1.5 \times 10^{-9} A/m^2$. The corrected and uncorrected Child-Langmuir screening distances are indicated above and are respectively: $D_s = 1.73$ m, $D_{CL} = 1.2$ m. The X and Z unit of distance is 1.0 meter.

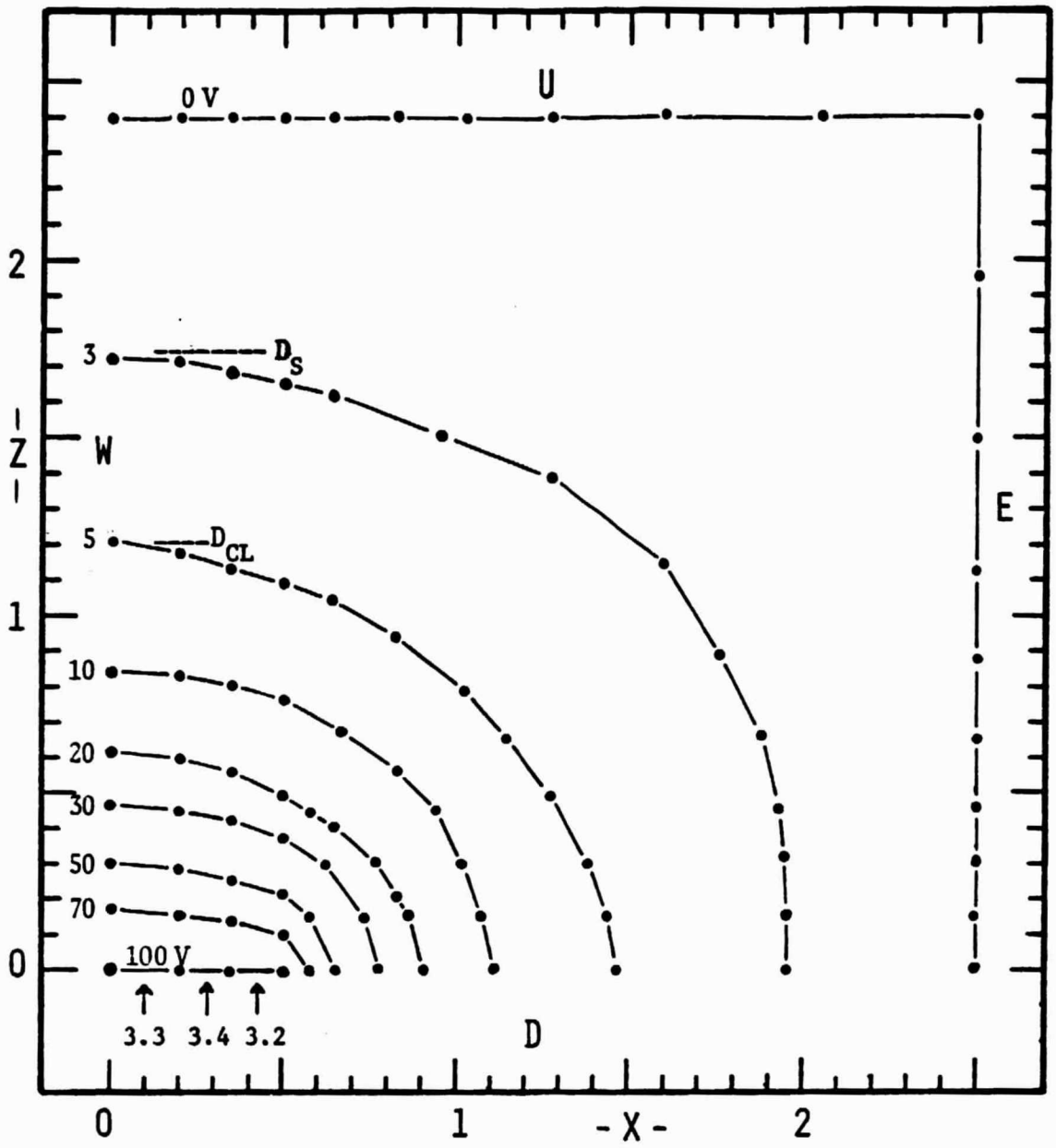

FIG.4/5,Model Pan36: The same panel and plasma of model Pan29 are modeled here with 90 grid points (not shown), and with a V = 0 boundary condition on both the UP and EAST boundaries. The distance unit is 1.0 meter.

FIG.4/6a

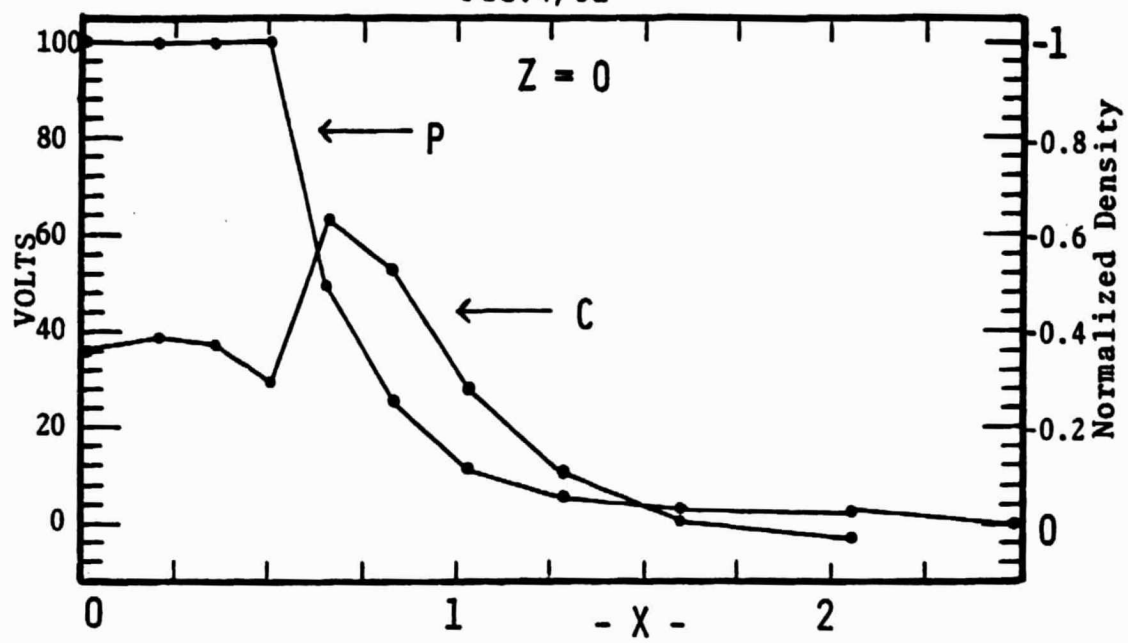

FIG.4/6b

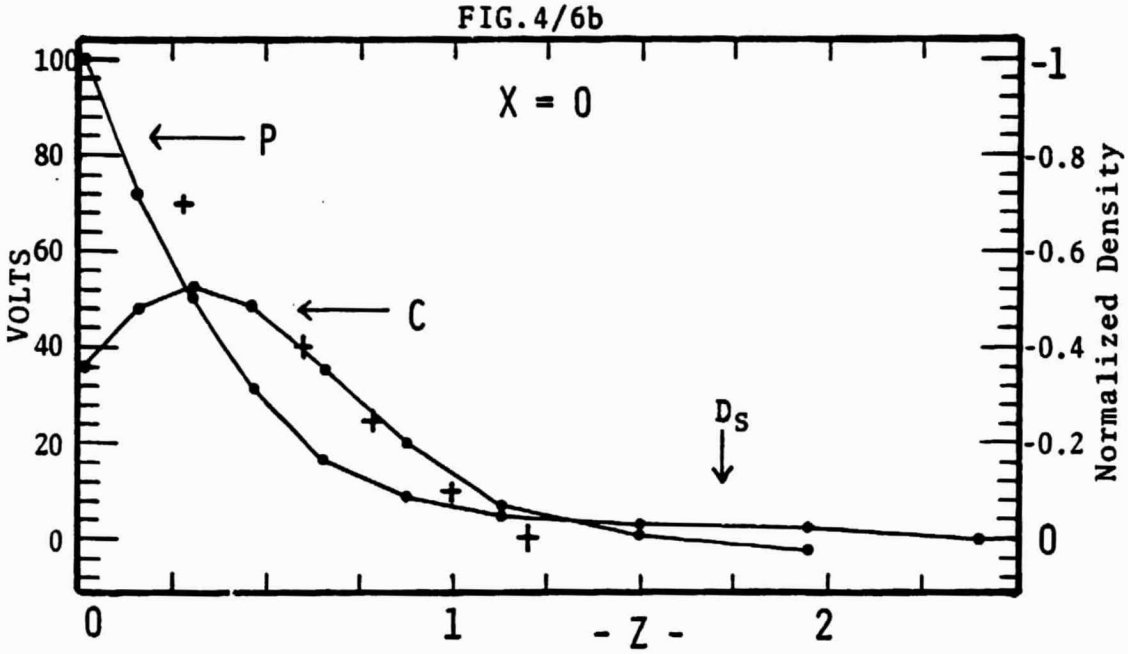

FIG.4/6: Potential (curve P) and charge density (curve C) profiles alonge the DOWN (4/6a) and WEST (4/6b) boundaries for the model Pan36. The density scale on the right is normalized to the ambient density, $N_o = 1.9 \times 10^4$/cc. In 4/6b, the Child-Langmuir potential profile is indicated by the unconnected crosses, and the initial velocity corrected C-L screening distance, D_s, is indicated by the arrow. The distance unit is 1.0 meter.

FIG.4/7a

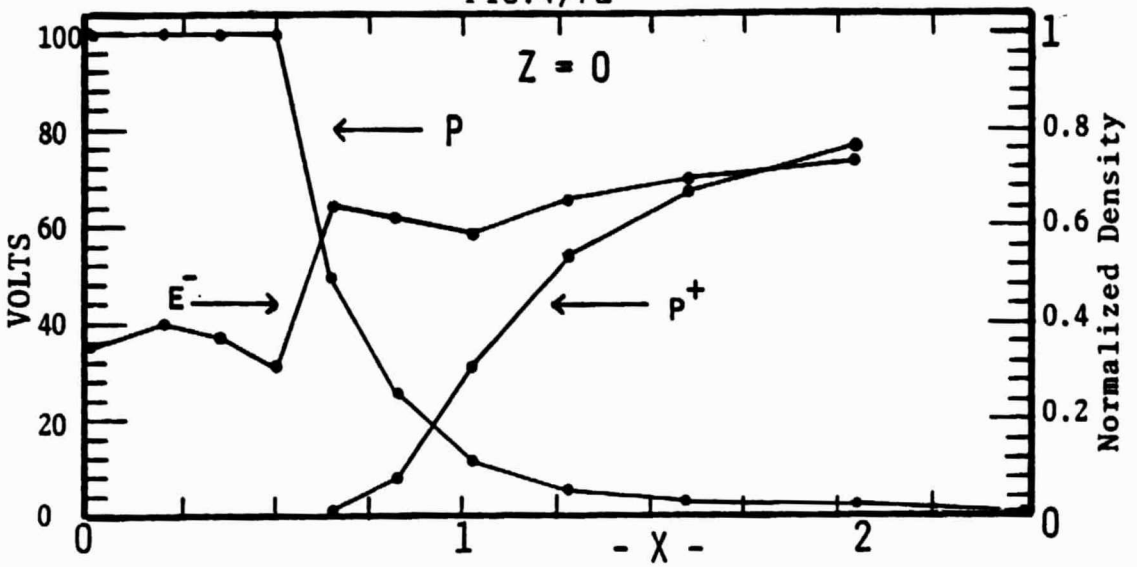

FIG.4/7b

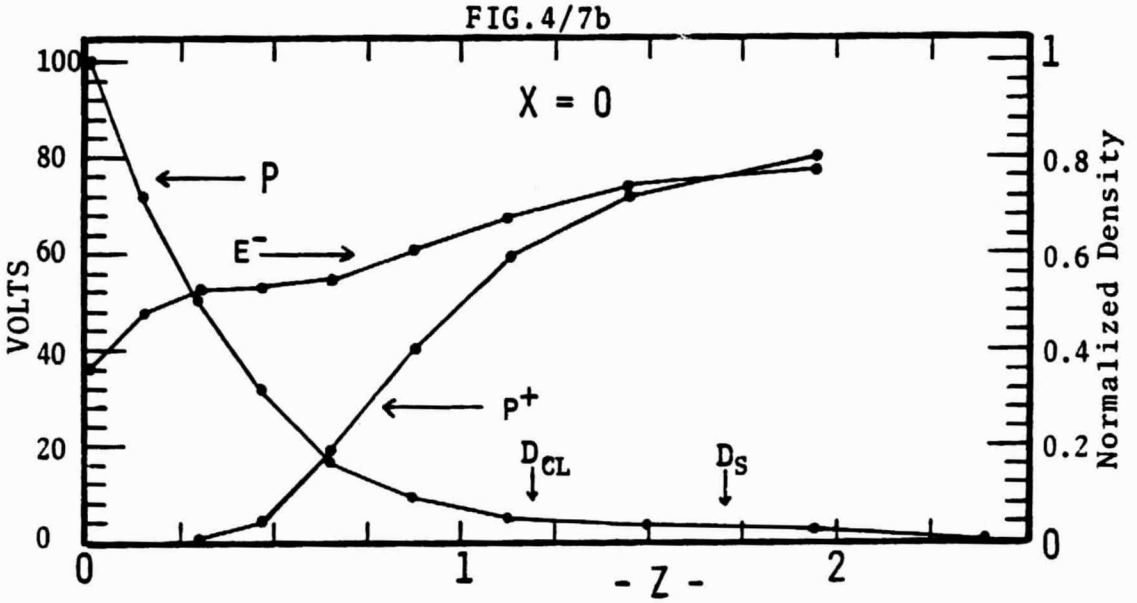

FIG.4/7: Potential (curve P), and electron and proton density profiles along the DOWN (4/7a) and WEST (4/7b) boundaries for the model Pan36. The corrected and uncorrected Child-Langmuir screening length estimates D_s and D_{CL} are indicated in 4/7b. The distance unit is 1.0 meter.